The Astrophysical Journal Supplement Series, 252:7 (23pp), 2021 January https://doi.org/10.3847/1538-4365/abc2c7

Proton and Hydrogen Transport through Hydrogen Environments: Ionization and Stripping

N. D. Cariatore[1] and D. R. Schultz[1,2]
[1] Department of Astronomy and Planetary Science, Northern Arizona University, Flagstaff, AZ 86001, USA; Nelson.Cariatore@nau.edu, David.Schultz@nau.edu
[2] Department of Applied Physics and Material Science, Northern Arizona University, Flagstaff, AZ 86001, USA
Received 2020 February 4; revised 2020 September 24; accepted 2020 September 26; published 2020 December 23

Abstract

Data are presented over a wide range of impact energies describing the ionization or stripping probability, projectile energy loss, and ejected electron and recoiling target energies and angles for proton and hydrogen passage through hydrogen astrophysical environments. These kinematic and reaction data are tabulated at three levels of detail for use in heavy-particle (H^+, H) and secondary-electron transport simulations: (1) the integral scattering cross section and average values of the distributions of energy and angle of the particles, (2) the singly differential cross sections as a function of particle energy and angle, and (3) a subset of the many possible doubly differential cross sections as functions of the particle energy and angle chosen to be most relevant to transport simulations.

Unified Astronomy Thesaurus concepts: Laboratory astrophysics (2004); Collision processes (2065); Interstellar medium (847); Stellar winds (1636); Supernova remnants (1667)

Supporting material: machine-readable tables

1. Introduction

The creation and use of models of astrophysical environments, as well as the interpretation of astrophysical observations, requires a significant amount, quality, and detail of information from laboratory astrophysics. Prominent examples include spectral lines and transition probabilities and electron, proton, and heavier-particle collision data. Availability of such data enables modeling of astrophysical emission and absorption, energy, momentum, and particle transport, as well as reactions.

Foundationally important for astrophysical applications, the target atom of greatest ubiquity is H, and therefore the dynamical problem of a proton or hydrogen atom colliding with atomic hydrogen is the simplest and best-studied heavy-particle atomic collision. Even so, data for $H^+ + H$ and $H + H$ in the literature, for the most part, have been largely incomplete with regard to coverage of relevant impact energies, reaction channels, and kinematics (e.g., availability of the cross-section differential in the scattering angle or energy loss of the projectile).

In ongoing work, here, and in previously published work, we seek to make available data that are as comprehensive as currently feasible for collisions relevant to ISM shocks, supernova remnants and bubbles, H I clouds, young stellar objects, winds within stellar spheres, and other astrophysical environments. The goal is to provide data covering the necessary wide range of energy- and charge-changing channels, collision energies, and most relevant scattering parameters. Recent examples of this work include data for elastic scattering of $H^+ + H$ (Schultz et al. 2016, and references therein) and $H + H$ (Ovchinnikov et al. 2017, and references therein). Here we add to the reactions considered by treating ionization of H by protons and H, as well as stripping (i.e., projectile ionization) of H by H impact.

The specific aims of the work are to provide data for all of the parameters of these reactions that can be of use in H^+, H, and secondary-electron transport simulations, yielding, for example, the diffusion of protons or H, their slowing down and angular scattering, and deposition of energy in ejected electrons, electronic excitation, and recoiling target ions or atoms. In addition, we have sought to compute these data with the greatest feasible accuracy and coverage of collision parameters.

Toward these ends, we present the results at three levels of detail, each suited to a level of complexity or completeness of a transport simulation. At the first level, we tabulate results for the integral cross section for ionization or stripping, which gives simulations the relative probability of these reactions, along with average values of the emerging particles' distribution of energies and scattering/emission/recoil angles. Adding the next level of detail, we present the singly differential cross sections (SDCS) that more completely characterize the particles' energies and angles. Finally, we have tabulated for dissemination via doi:10.7910/DVN/GN5SKT a subset of the many possible doubly differential cross sections (DDCS) as simultaneous functions of the particles' energies and angles, chosen as being the most likely of them to be of use in simulations going to this level of description of the particles' kinematics.

An example of the use of integral and differential cross sections (Schultz et al. 2017, 2019) in transport simulations is work undertaken to describe X-ray, IR photon, and secondary-electron production from ion precipitation at Jupiter carried out in support of Juno observations and Jovian magnetosphere–atmosphere coupling modeling (Ozak et al. 2013; Houston et al. 2018, 2020). Integral cross sections computed for oxygen and sulfur ions for the elastic scattering and inelastic channels (target ionization, projectile stripping, charge transfer, and target and projectile excitation) have been used to determine the reaction probabilities for ion charge change (including subsequent photon emission probabilities and spectra) along the precipitating ion trajectory through the atmosphere. The

differential cross sections yield the energy loss to determine the slowing down of the ion along the trajectory, as well as the emission angle and energy distribution of the secondary electrons produced, contributing to atmospheric electron currents and IR emission from excitation of H_2. The transport simulation also yields quantities such as the stopping power and ion charge state distribution that were used to validate the very large underlying atomic data set through comparison with existing measurements.

After description of the theoretial method (Section 2), we present data for ionization in proton collisions with H (Section 3), ionization and stripping in H + H (Section 4), and simultaneous ionization and stripping in H + H (Section 5).

2. Theoretical Method

Though collisions of protons and H with H are among the most fundamental atomic collision systems, involving just one or two electrons and two nuclei ("centers"), accurate theoretical treatments capable of describing the reaction probabilities and kinematics of all of the particles in the collision are to this day limited. For very high impact energies, perturbation theory may be applied to solve the underlying dynamical equation (the one- or two-electron, two-center Schrödinger equation), but at intermediate and low impact energy, such methods are not as applicable and coupled equations solution of the Schrödinger equation is required (involving expansion of the wave function either in atomic orbitals and continuum states on one or both centers at intermediate collision energy or in molecular orbitals at low energy).

In addition, measurements of the properties of these collisions, which would provide important benchmarks for theory, are rare owing to the experimental challenges of producing ground-state, dissociated atomic hydrogen from H_2. Fortunately, measurements exist for the integral ionization cross section over a reasonably wide energy range and for the singly differential cross section as a function of ejected electron energy and angle for $H^+ + H$, and over a more narrow range of energies for the integral cross section for H + H, to provide important comparisons with results of theoretical approaches that may provide much more comprehensive and detailed data.

Therefore, here we adopt a theoretical method capable of providing a reasonable treatment of electron removal from either the target H atom (ionization) or the projectile H atom (stripping) over the range of some hundreds of eV to tens of MeV, which provides an explicit description of the kinematics of all of the particles in the collision, the classical trajectory Monte Carlo (CTMC) method. Further, in the high-energy regime for $H^+ + H$, in which CTMC underestimates the probability of ionization, we use perturbation theory to restore the missing portion, and at low energy, where CTMC also underestimates the probability of ionization, we normalize the cross sections to recommended values, as described subsequently.

The CTMC method, in brief, simulates an atomic collision by sampling trajectories evolving from initial electronic orbits within a large ensemble of configurations chosen to mimic the corresponding quantum electronic position and momentum distributions (Abrines & Percival 1966; Olson & Salop 1977). The motion of the particles is determined by an iterative numerical solution of Newton's or Hamilton's equations of motion. At an asymptotic final distance, the classical binding energies are then calculated to determine whether an inelastic event occurred.

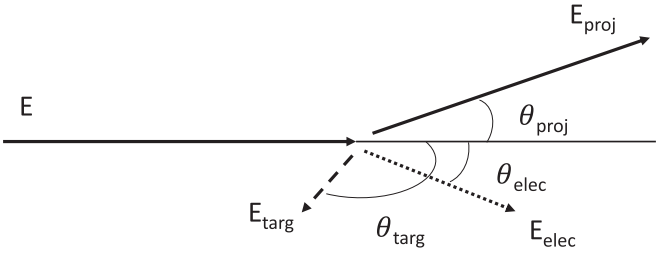

Figure 1. Illustration of the energies and angles of scattering/emission/recoil of the particles for ionization in H^+, H + H.

From this we may derive the reaction probability (characterized by the integral cross section) and the energy and scattering/emission/recoil angles of the particles—projectile, target nucleus, and electron (characterized by either their average value or the singly or doubly differential cross sections). Results of this method have been critically compared regarding the production of secondary electrons with measurements and other theoretical methods for a wide variety of atomic collisions, for example, for proton (Kerby et al. 1995) and He^+ (Hsu et al. 1996) impact of H; fluorine ions colliding with H_2 (Reinhold et al. 1991); C^+ (Toburen et al. 1990), F^{9+} (Schultz & Reinhold 1994), and highly charged gold ion (Sataka et al. 1994) impact of He; and carbon ion impact of neon (Toburen et al. 2006).

In addition, in the data tables presented here, all integral and differential cross sections calculated are normalized to recommended values that have been created taking into account the most reliable measurements and theoretical results at the time of the evaluation leading to them. Therefore, the intrinsic energy range of applicability of the CTMC calculations (20–300 keV), plus the additional correction from quantum mechanical perturbation theory described below for $H^+ + H$ (300 to 10,000 keV), is extended through this normalization.

2.1. pCTMC

The most frequently employed variant of the CTMC method is the original formulation (Abrines & Percival 1966; Olson & Salop 1977) that reproduces exactly (within the Monte Carlo statistics of the initial ensemble of orbits) the electronic momentum distribution of H. This variant is denoted pCTMC ("p" for reproducing the electronic momentum distribution exactly) and is based on selection of initial orbits from the microcanonical distribution. Consequently, all orbits have the same, "on-shell" energy, 13.6 eV, equal to the binding energy of H. While the atomic hydrogen electronic momentum distribution is reproduced, the electronic radial distribution is classically cut off at 2 Bohr radii. Particularly at intermediate collision energies, roughly comparable to the mean orbital electron velocity (for H^+ or H + H, roughly 25–200 keV), ionization is generally described well by this model because of the importance of the correct binding energy and momentum distribution for the range of impact parameters that predominantly contribute to electron emission.

2.2. First-order Born Approximation Correction

However, for charged projectiles, at high impact energies (200 keV and above for $H^+ + H$), CTMC increasingly underestimates the ionization probability owing to the lack of dipole-like, low momentum transfer transitions to the

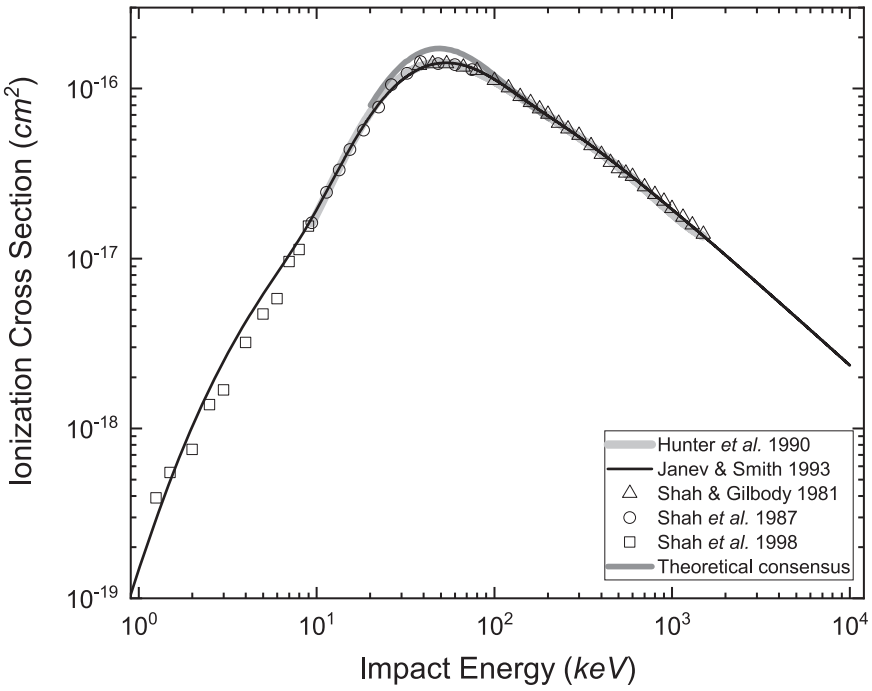

Figure 2. Recommended values of the integral cross section for ionization in $H^+ + H$ (Hunter et al. 1990; Janev & Smith 1993) displayed along with the foundational measurements from the Queen's University Belfast (Shah & Gilbody 1981; Shah et al. 1987, 1998). As explained in the text, the figure also displays a curve representing a consensus of more recent theoretical treatments that disagree with the measurements around the peak of cross section.

continuum. These transitions contribute almost entirely to emission of low-energy, largely isotropically emitted electrons, representing an important contribution to both the integral and differential cross sections for electron emission. It has been shown (Reinhold & Bürgdorfer 1993; Kerby et al. 1995) that these portions of the cross section may be added to the CTMC results by use of quantum mechanical perturbation theory (in particular, via an appropriate modification of the first-order Born approximation). Recent work that illustrates the application of this correction has been published for fully and partially stripped oxygen ion impact of molecular hydrogen ($O^{0\text{-}8+} + H_2$; Schultz et al. 2017, 2019) and hydrogen impact of molecular hydrogen ($H^{-1,0,1+} + H_2$; Schultz et al. 2020) relevant to ion precipitation into Jupiter's upper atmosphere.

Therefore, for high-energy $H^+ + H$ collisions, we add the first-order Born correction (B1C) to the integral and differential cross sections computed with pCTMC. Calculated as an integral cross section, the correction has been added directly to the CTMC result. Similarly, the correction, calculated as the SDCS as a function of ejected electron energy ($E_{\rm elec}$) and angle ($\theta_{\rm elec}$), has been added directly to the corresponding SDCS from CTMC. For the other SDCS (as functions of $\theta_{\rm proj}$, $E_{\rm targ}$, and $\theta_{\rm targ}$), the energy loss, and the DDCS, we convert the B1C DDCS ($E_{\rm elec}$, $\theta_{\rm elec}$) into events that may be added to the CTMC-generated events. This may be done since the SDCS, divided by the integral cross section, is proportional to the number of events for the CTMC calculations. Relationships between $E_{\rm elec}$ and $\theta_{\rm elec}$ and the other parameters, given below, allow events to be generated describing all of the kinematic parameters so we can add them to CTMC events.

1. From the theory describing the B1C (Reinhold & Bürgdorfer 1993), the impact parameter range associated with this correction may be estimated, and from that the total number of events to be added to those from CTMC may be computed from the B1C and CTMC integral cross sections.
2. Sampling of the B1C DDCS ($E_{\rm elec}$,$\theta_{\rm elec}$) is used to generate events with $E_{\rm elec}$ and $\theta_{\rm elec}$ proportional to the cross section.
3. From the generated event an energy loss is calculated using $E_{\rm elec}$ and the ionization potential, plus a small shift of less than 1 eV that facilitates the solution of the expression (see Section 3 below) connecting the energy loss and the projectile scattering angle, thus deriving $\theta_{\rm proj}$.
4. Finally, $E_{\rm targ}$ and $\theta_{\rm targ}$ are found from momentum balance with $E_{\rm proj}$, $\theta_{\rm proj}$, $E_{\rm elec}$, and $\theta_{\rm elec}$.

From the sum of the CTMC and B1C-generated events we may then bin the SDCS and DDCS and compute the kinematic parameter averages.

The B1C added to the CTMC results brings the sum into good agreement with the recommended integral cross section for energies greater than 300 keV, and then the overall normalization of the CTMC+B1C results is made across the entire energy range from threshold to 10 MeV. Since the B1C decreases with decreasing impact energy and becomes very small for energies less than about 300 keV, the correction adds quite smoothly to CTMC in that range of energies.

2.3. rCTMC

At low to intermediate collision energy CTMC also underestimates the ionization probability. This may be partially ameliorated by use of another variant that reproduces the electronic radial distribution for H, at the expense of requiring a distribution of "off-shell" orbital energies (Hardie & Olson 1983; Cohen 1985), denoted rCTMC ("*r*" for reproducing the electronic radial distribution). Ionization in events with initial orbits with lower binding energy (and corresponding larger

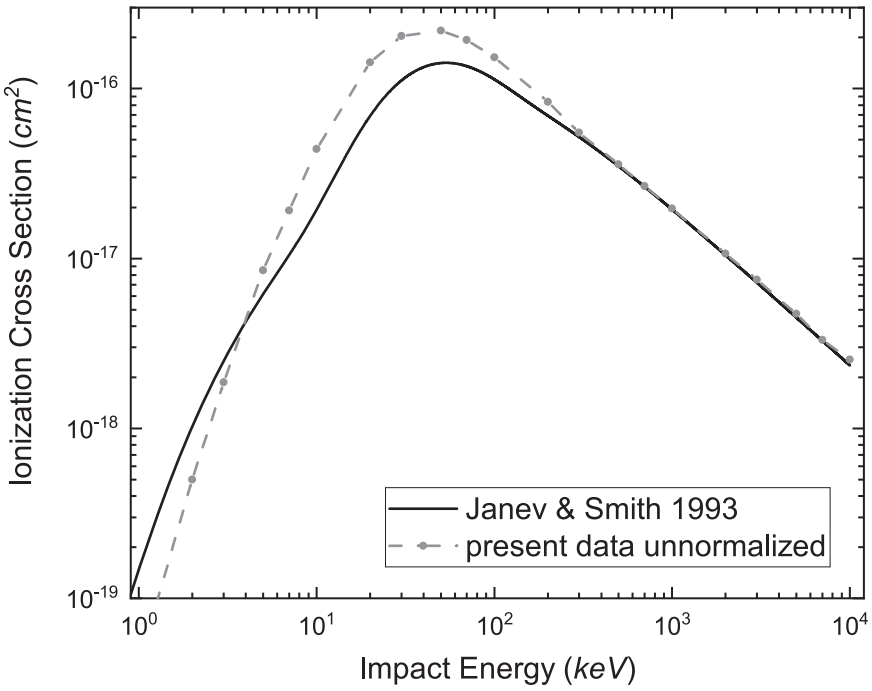

Figure 3. Comparison of the present calculations and the IAEA recommendation for ionization in $H^+ + H$ collisions. As described in the text, all integral and differential cross sections for $H^+ + H$ are normalized to the IAEA recommended curve in the tabulated data.

radial extent) mimics some of the quantum mechanical transitions to the continuum not represented well in pCTMC.

2.4. Collision Kinematics

At the most fundamental level, a transport simulation describing H^+, H passing through a gas of H requires the integral cross section, σ_α, for each of the dominant reaction channels, α (e.g., elastic scattering, ionization, excitation, charge transfer), in order to choose at any given point which channel to follow. This may be accomplished by calculating the mean free path, $\lambda_\alpha = \rho_H/\sigma_\alpha(E)$, where ρ_H is the density of H through which the projectile propagates and E is the collision energy in the laboratory frame. (All particle energies and angles are given in this work in the laboratory frame of reference with respect to the initial target H.)

At the next level, a transport simulation would want to track the energy loss of the projectile, since the probability of each channel occurring at the next collision is a function of E. The energy loss (or gain) may be obtained from conservation of energy, that is, by subtracting from E the energy transferred into each of the particles by the collision. For elastic scattering, the energy lost by the projectile is transferred into the recoil of the target and may be given to good approximation by

$$E_{\rm loss}^{\rm elas} = E - E\cos^2(\theta_{\rm proj}). \quad (1)$$

For an inelastic collision, such as for ionization considered here, the inelasticity should be added to this elastic energy-loss formula, that is,

$$E_{\rm loss}^{\rm ioniz} = E\,(1 - \cos^2(\theta_{\rm proj})) - E_{\rm elec} - {\rm IP}, \quad (2)$$

where IP is the ionization of the target, here that of H.

Alternatively, the explicit energies of each particle emerging from the collision could be computed in the CTMC approach and subtracted from the incident energy to find the energy loss, or the difference between the incident and outgoing energy of the projectile to give the energy loss. We find that the energy loss given by Equation (2) provides a numerically less "noisy" value, owing to the inherent numerical errors in the integration of the equations of motion of the particles in the CTMC method.

Beyond the probability of each channel occurring and the energy loss of the projectile, transport simulations at a greater level of detail may incorporate knowledge of energies and scattering/emission/recoil angles of all of the particles emerging from the collision. These angles and energies are illustrated for the ionization channel in Figure 1. While the CTMC calculations also give the azimuthal angles, we do not capture this information in the present work, as a judgment must be made as to the level of detail of the data provided for simulations that could be handled, as well as at what level the data would be of the highest priority of use. We also report results (average energies and angles, SDCS) in an uncorrelated manner. That is, particle energies and angles are correlated with one another (e.g., a propensity for recoil of the target opposite scattering of the projectile). These correlations are reflected in higher levels of differential cross sections, for example, DDCS describing how two of the kinematic parameters are distributed jointly. Again, providing all of the possible DDCS (or higher, such as triply differential cross sections, quadruply differential cross sections, etc.) would entail enormous data sets that transport simulations would have to manage.

2.5. Notes on Use of the Tabulated Data

The singly and doubly differential cross sections calculated here integrate to the corresponding integral cross section tabulated, within an error resulting from the varying statistical uncertainty in the Monte Carlo calculations. That is, for

Table 1
Integral Cross Section (Denoted "TCS" for Total Cross Section) along with the Average Values of the Kinematic Parameters of the Collision for Ionization in $H^+ + H$ as a Function of Laboratory Collision Energy from Ionization Threshold to 10 MeV

Energy (keV)	TCS (cm^2)	$\langle E_{loss}^{ioniz} \rangle$ (eV)	$\langle \theta_{proj} \rangle$ (deg)	$\langle E_{elec} \rangle$ (eV)	$\langle \theta_{elec} \rangle$ (deg)	$\langle E_{targ} \rangle$ (eV)	$\langle \theta_{targ} \rangle$ (deg)
1.36E–02	1.00E–99	1.36E+01	1.80E+02	1.00E–99	9.00E+01	1.36E+01	1.00E–99
2.00E–02	2.00E–29	2.00E+01	1.55E+02	8.00E–02	8.90E+01	2.80E+01	1.00E–02
3.00E–02	4.00E–27	3.00E+01	1.30E+02	3.00E–01	8.80E+01	4.00E+01	1.00E+00
5.00E–02	9.00E–25	5.00E+01	1.00E+02	5.00E–01	8.65E+01	5.50E+01	1.00E+01
7.00E–02	6.00E–24	7.00E+01	8.00E+01	6.00E–01	8.55E+01	6.50E+01	2.00E+01
1.00E–01	4.00E–23	7.80E+01	6.00E+01	7.00E–01	8.40E+01	7.00E+01	3.00E+01
2.00E–01	5.01E–22	7.32E+01	3.23E+01	8.90E–01	8.27E+01	6.01E+01	5.56E+01
3.00E–01	2.22E–21	4.64E+01	1.76E+01	1.03E+00	8.61E+01	3.53E+01	6.96E+01
5.00E–01	1.40E–20	2.10E+01	5.16E+00	1.14E+00	7.30E+01	9.27E+00	7.81E+01
7.00E–01	4.54E–20	1.91E+01	3.29E+00	1.29E+00	6.85E+01	6.21E+00	7.84E+01
1.00E+00	1.47E–19	1.81E+01	2.35E+00	1.47E+00	6.70E+01	5.20E+00	7.88E+01
2.00E+00	1.03E–18	1.70E+01	9.71E–01	2.00E+00	5.91E+01	2.38E+00	7.77E+01
3.00E+00	2.50E–18	1.65E+01	5.40E–01	2.20E+00	5.16E+01	1.22E+00	7.54E+01
5.00E+00	6.14E–18	1.64E+01	2.47E–01	2.48E+00	4.68E+01	5.12E–01	7.31E+01
7.00E+00	1.05E–17	1.68E+01	1.47E–01	3.00E+00	3.83E+01	2.56E–01	7.31E+01
1.00E+01	1.93E–17	1.76E+01	8.36E–02	3.96E+00	3.09E+01	1.39E–01	7.59E+01
2.00E+01	6.91E–17	2.07E+01	3.35E–02	7.06E+00	2.75E+01	5.70E–02	8.89E+01
3.00E+01	1.12E–16	2.31E+01	2.47E–02	9.52E+00	2.97E+01	3.98E–02	9.55E+01
5.00E+01	1.41E–16	2.69E+01	1.93E–02	1.33E+01	3.47E+01	3.60E–02	1.00E+02
7.00E+01	1.36E–16	2.96E+01	1.68E–02	1.60E+01	3.90E+01	3.61E–02	1.02E+02
1.00E+02	1.13E–16	3.25E+01	1.46E–02	1.88E+01	4.41E+01	4.01E–02	1.02E+02
2.00E+02	6.93E–17	3.75E+01	1.10E–02	2.39E+01	5.44E+01	3.86E–02	1.01E+02
3.00E+02	5.52E–17	4.10E+01	9.22E–03	2.74E+01	5.94E+01	3.28E–02	9.21E+01
5.00E+02	3.58E–17	4.24E+01	7.36E–03	2.88E+01	6.66E+01	2.82E–02	9.70E+01
7.00E+02	2.67E–17	4.34E+01	6.10E–03	2.98E+01	7.07E+01	2.59E–02	9.75E+01
1.00E+03	1.97E–17	4.44E+01	5.04E–03	3.07E+01	7.40E+01	2.14E–02	9.70E+01
2.00E+03	1.07E–17	4.62E+01	3.59E–03	3.26E+01	7.92E+01	1.87E–02	9.49E+01
3.00E+03	7.49E–18	4.73E+01	2.90E–03	3.36E+01	8.14E+01	2.18E–02	9.36E+01
5.00E+03	4.73E–18	4.86E+01	2.21E–03	3.50E+01	8.36E+01	1.57E–02	9.24E+01
7.00E+03	3.32E–18	4.93E+01	2.07E–03	3.57E+01	8.48E+01	4.48E–02	9.18E+01
1.00E+04	2.54E–18	5.01E+01	1.51E–03	3.65E+01	8.57E+01	1.26E–02	9.13E+01

(This table is available in its entirety in machine-readable form.)

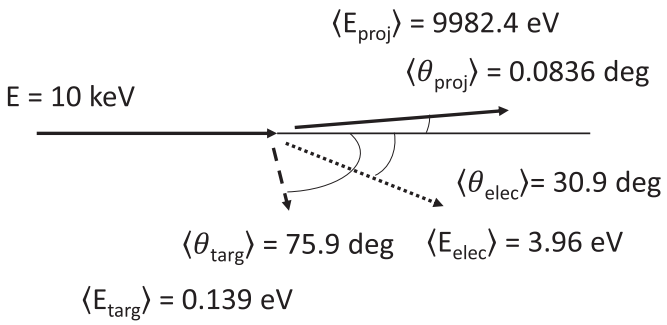

Figure 4. Illustration of the average values of the kinematic parameters for $E = 10$ keV for ionization in $H^+ + H$ collisions (vectors and angles not to scale).

example, for the SDCS as a function of scattering, recoil, or emission angle

$$\sigma = \int d\sigma/d\Omega \; d\Omega, \tag{3}$$

where the solid-angle differential is $d\Omega = 2\pi \sin(\theta) \; d\theta$. Transport simulations using the differential cross sections should sample $d\sigma/d\Omega = d\sigma/d\ \theta/(2\pi \sin(\theta))$ in order to have the distribution of events match that given by the corresponding differential and integral cross section, in the limit of a sufficiently large number of samples.

The user of the tabulated data will also notice that the SDCS and DDCS have entries that are zero, denoted here with a series of dots. As with any Monte Carlo method, CTMC has a zero quantization whenever no simulation events occur. Also, in order to avoid tabulation of cross sections with large statistical uncertainties, we display a number only if five or more simulation events occur. Therefore, the user of the data will require some strategy to fill in the missing values to enable interpolations of the data.

The missing values occur either at the extremes of the tabulated results for a given parameter—for example, at the lower end of the values tabulated for the ejected electron energy or at its upper end—or at intermediate values. When they occur at the extremes, it is most likely physically that the cross section is dropping off rapidly, and we suggest inserting entries that decline to a very small value in just a small number of steps, for example, 10^{-30}, 10^{-40}, 10^{-99}. When they occur at intermediate values, it is most likely physically that there is a

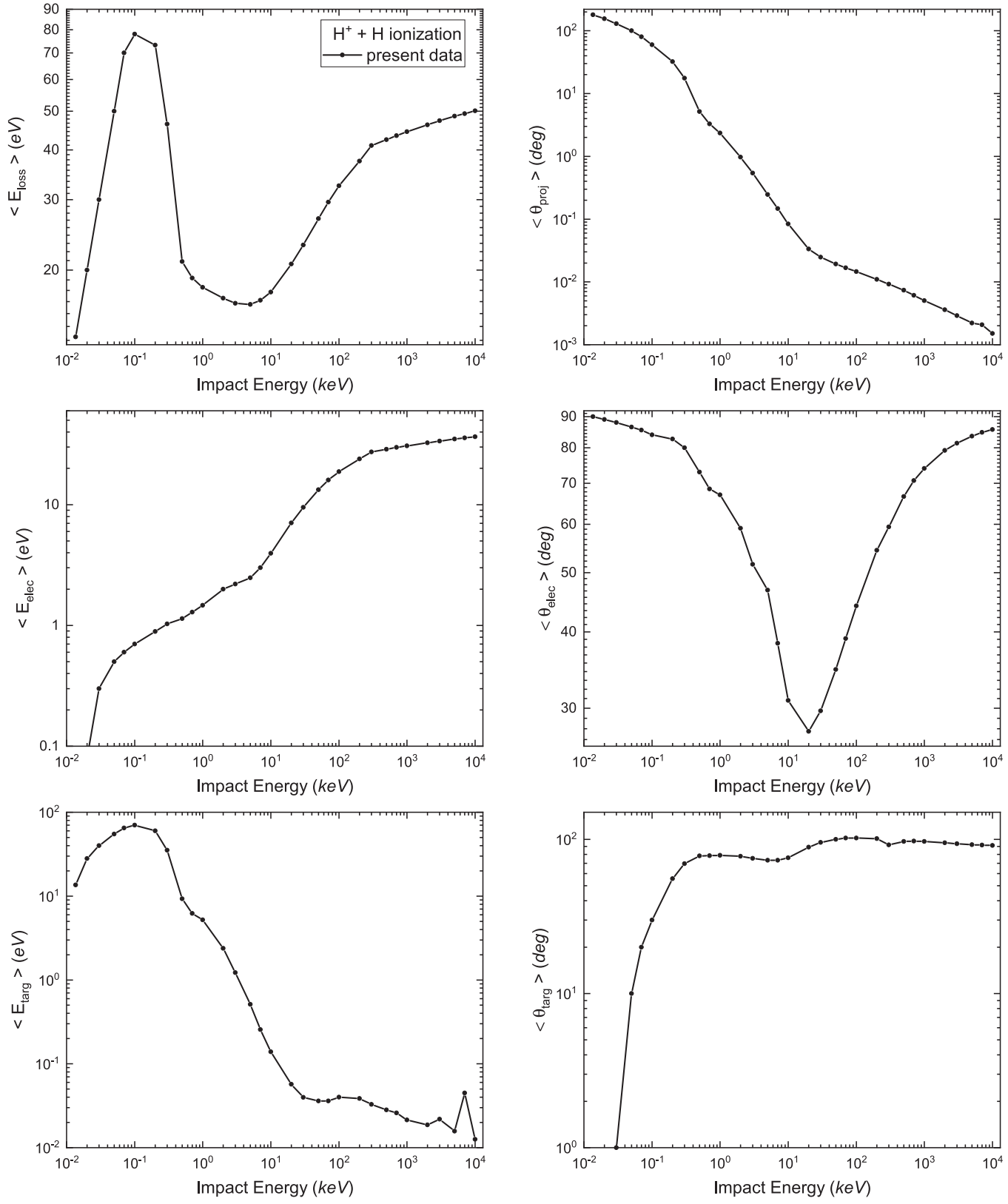

Figure 5. The six kinematic parameters as a function of impact energy for ionization in $H^+ + H$.

minimum just below the quantization of the Monte Carlo results we have been able to obtain. A reasonable strategy in such cases would be to insert one (or more if there are several missing entries) value that is, say, a factor of 10 smaller than the nonzero values on either side of the missing value (or values).

Table 2
SDCS and Projectile Energy Loss as Functions of θ_{proj}, E_{elec}, θ_{elec}, E_{targ}, and θ_{targ} for Ionization in H^+ Impact on H

E_{imp} (keV)	θ_{proj} (deg)	$E_{loss}(\theta_{proj})$ (eV)	SDCS(θ_{proj}) (cm^2 sr^{-1})	E_{elec} (eV)	SDCS(E_{elec}) (cm^2 eV^{-1})	θ_{elec} (deg)	SDCS(θ_{elec}) (cm^2 sr^{-1})	E_{targ} (eV)	SDCS(E_{targ}) (cm^2 eV^{-1})	θ_{targ} (deg)	SDCS(θ_{elec}) (cm^2 sr^{-1})
5.00E-01	1.50E+00	1.45E+01	1.23E-18	3.00E-02	1.63E-20	4.50E+00	1.11E-20	3.00E-01	6.33E-21	5.75E+01	1.41E-22
⋯	2.50E+00	1.57E+01	7.08E-19	7.50E-02	1.57E-20	7.50E+00	1.01E-20	7.50E-01	6.02E-21	6.25E+01	2.38E-22
⋯	3.50E+00	1.71E+01	2.59E-19	3.00E-01	9.12E-21	8.50E+00	9.32E-21	3.00E+00	1.26E-21	6.75E+01	4.54E-22
⋯	4.50E+00	1.80E+01	1.46E-19	7.50E-01	6.00E-21	9.50E+00	9.94E-21	6.25E+00	3.52E-22	7.25E+01	2.41E-21
⋯	5.50E+00	1.95E+01	8.65E-20	3.00E+00	1.41E-21	1.10E+01	6.36E-21	8.75E+00	2.38E-22	7.75E+01	1.31E-20
⋯	6.50E+00	2.26E+01	5.04E-20	6.25E+00	7.01E-23	1.30E+01	4.52E-21	1.25E+01	1.24E-22	8.25E+01	9.41E-21
⋯	7.50E+00	2.42E+01	3.71E-20	⋯	⋯	1.50E+01	3.59E-21	1.75E+01	5.02E-23	⋯	⋯
⋯	8.50E+00	2.60E+01	2.62E-20	⋯	⋯	1.70E+01	6.27E-21	2.50E+01	2.95E-23	⋯	⋯
⋯	9.50E+00	2.76E+01	1.50E-20	⋯	⋯	1.90E+01	4.24E-21	4.00E+01	1.42E-23	⋯	⋯
⋯	1.10E+01	3.64E+01	7.65E-21	⋯	⋯	2.25E+01	3.23E-21	6.00E+01	8.22E-24	⋯	⋯

(This table is available in its entirety in machine-readable form.)

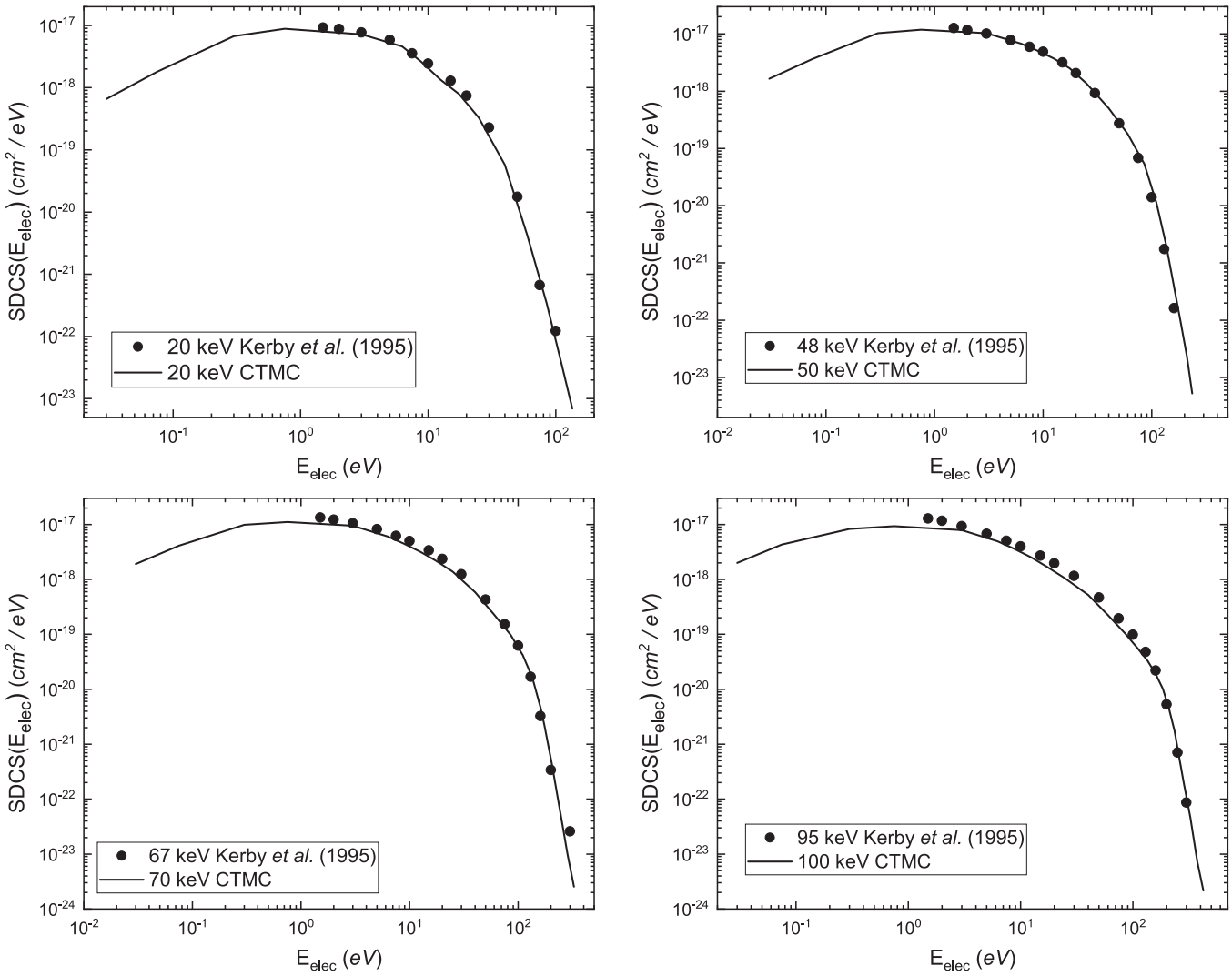

Figure 6. Comparison of the present calculations of the singly differential cross section as a function of ejected electron energy with the measurements of Kerby et al. (1995).

3. $H^+ + H$ Ionization

Owing to its fundamental nature, a significant number of measurements of the $H^+ + H$ ionization cross section exist, as well as many theoretical treatments. Therefore, recommended values for this integral cross section have been created, for example, because of the importance of this process in fusion energy research. Figure 2 shows two of the recommended cross sections as a function of incident proton laboratory energy given by the fusion energy data center at Oak Ridge National Laboratory (Hunter et al. 1990) and the Atomic and Molecular Data Center at the International Atomic Energy Agency (IAEA; Janev & Smith 1993). Also shown are the measurements generally judged to be the most reliable (which largely underpin the recommended values) from the Queen's University Belfast (Shah & Gilbody 1981; Shah et al. 1987, 1998).

Subsequent to the last of the foundational measurements of this fundamentally important cross section, a number of "modern" theoretical methods have found a ∼15% disagreement with the measurements around the peak of the cross section. These methods include the Gaussian atomic-orbital close-coupling method (Toshima 1999), the finite-element and Fourier collocation lattice, time-dependent Schrödinger equation methods (Kołakowska et al. 1999), the grid-based momentum space method (Sidky & Lin 2001), the Sturmian atomic-orbital close-coupling method (Winter 2009), and the two-center convergent close-coupling method (Abdurakhmanov et al. 2018). Therefore, we include in Figure 2 a thick curve illustrating a value representing the consensus of our judgment of the most reliable of these modern theoretical results, largely following the latest of these from the work of Abdurakhmanov et al. (2018).

In comparison, the results from the present work are shown along with the most recent recommended value (Janev & Smith 1993) in Figure 3. The CTMC results are from the rCTMC method for $E \leqslant 200$ keV, from pCTMC for $E > 200$ keV, and including the B1C for $E > 200$ keV. Here we adopt the IAEA recommended cross section, normalizing the present theoretical integral and differential cross sections to the recommendation, which is reflected in the values of the integral cross section given in Table 1. Should future work revise the recommendation based on further theoretical or experimental measurements in the region around the peak of the cross section, following, for example, the present theoretical consensus shown in Figure 2, all normalizations here

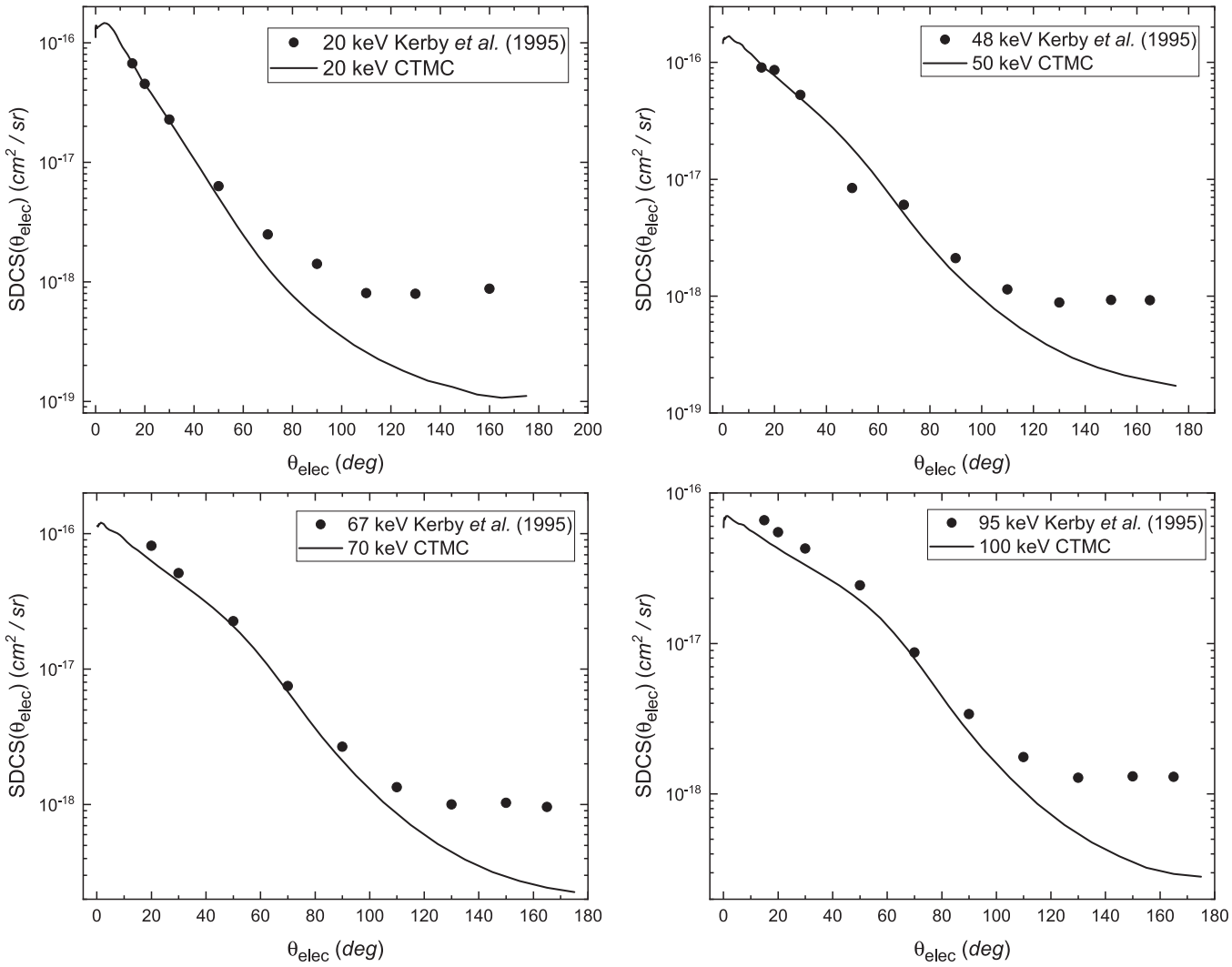

Figure 7. Comparison of the present calculations of the singly differential cross section as a function of ejected electron angle with the measurements of Kerby et al. (1995).

can be changed by the user of the data to the revised recommendation.

Also shown in Table 1 are the average values of the particle energies and angles and the energy loss as computed via Equation (2). These are provided not only to illustrate in a compact way the distributions of these kinematic parameters but also because transport simulations may use these rather than the more detailed full distributions (given in Table 2 by the tabulated singly differential cross sections and as made available via doi:10.7910/DVN/GN5SKT for a subset of the many doubly differential cross sections).

Figure 4 illustrates these average values for a laboratory-frame impact energy of 10 keV. As typical for the higher impact energies considered, the figure shows that the projectile scattering angle is generally small, and so the energy loss is generally small and is dominated by the inelastic component. Values of the average energies show that the projectile's energy loss is equal to the sum of the kinetic energies of the recoiling target and ejected electron plus the hydrogen ionization potential (13.6 eV). Also of note is the correlation of the recoil and electron energy and angle in momentum balance with the projectile's.

Results have been calculated for the lowest impact energy feasible with the CTMC method, 200 eV, that is, for an impact energy for which a sufficient number of ionization events are obtained by this Monte Carlo method to provide reasonable statistical uncertainty in the integral cross section and kinematic parameters. Below this energy we have extrapolated the integral cross section and kinematic parameters down to the ionization threshold. Thus, Table 1 provides results between 13.6 eV and 10 MeV, covering the range of energies characterizing many astrophysical environments.

Figure 5 shows the behavior as a function of impact energy of all six kinematic parameters for ionization in $H^+ + H$. For example, the figure shows that at low impact energy the average scattering angle of the projectile is greatest. In this energy range a close interaction with the electron is required to eject it, and the nearness to the target nucleus also results in significant deflection due to the nearly Coulombic projectile–target nucleus scattering at small impact parameters. The average projectile scattering angle decreases as impact energy increases, as larger impact parameters, with a less central collision with the target nucleus, and with greater incident momentum, contribute to the overall ionization of the target.

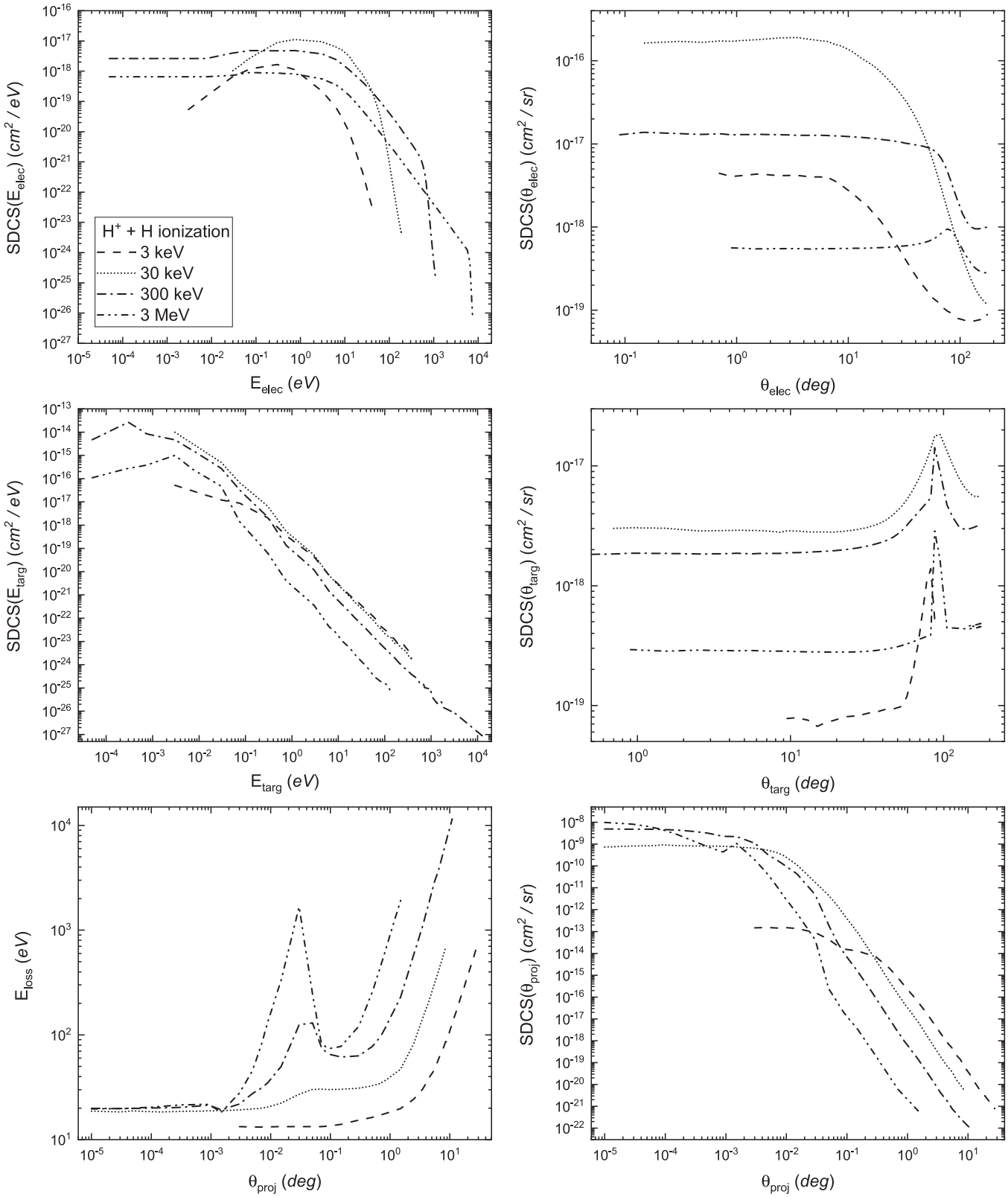

Figure 8. Illustration of all of the singly differential cross sections for a representative set of energies (3, 30, 300, and 3000 keV) spanning the impact energy range considered here for $H^+ + H$ collisions.

Correlated with this behavior of $\langle\theta_{\rm proj}\rangle$, the $\langle E_{\rm elec}\rangle$ is small at low impact energy because the projectile has less energy to impart to it given the large energy loss due to the scattering (and transfer to the recoiling target) and the need to transfer at least a kinetic energy equivalent to the ionization potential to eject the electron. As impact energy increases, more projectile energy is available to transfer to the ejected electron and $\langle E_{\rm elec}\rangle$ increases. For low E, the electron is ejected largely

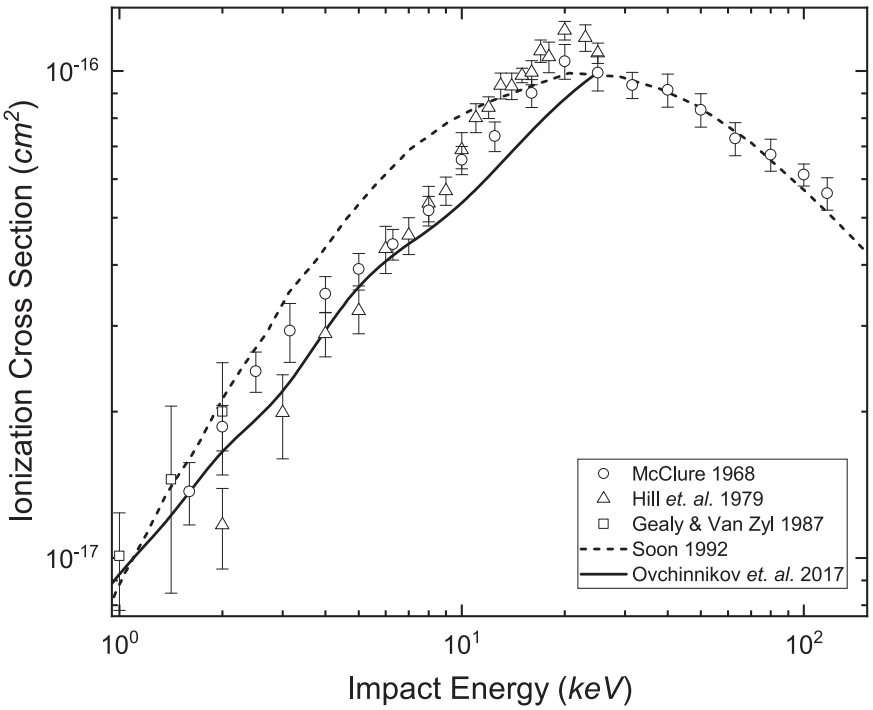

Figure 9. Comparison of the existing measurements (McClure 1968; Hill et al. 1979; Gealy & Van Zyl 1987) of the integral cross section for ionization in H + H with the theoretical results of the classical impulse approximation (Soon 1992) and the advanced adiabatic method (Ovchinnikov et al. 2017) in the energy range around the peak of the cross section.

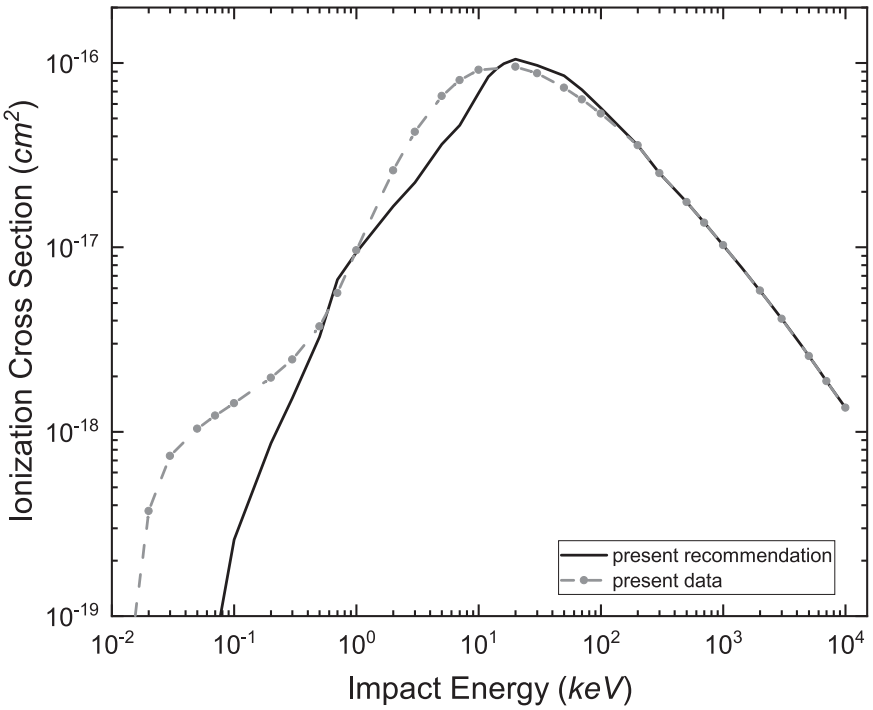

Figure 10. Comparison of the present calculations with the present recommended curve as described in the text, for ionization (or stripping) in H + H. All integral and differential cross sections tabulated are normalized to the recommended curve.

isotropically, but with a bias toward 90° relative to the incident projectile momentum vector, resulting in a $\langle\theta_{\rm elec}\rangle$ near 90°. For larger E, the electron tends to be pulled toward the receding projectile after ejection, leading to a smaller $\langle\theta_{\rm elec}\rangle$, and at high impact energy, the electron is dominantly ejected at 90° when the projectile moves swiftly by the target.

Correlated to the projectile scattering and electron ejection, the average energy of the recoiling target $\left\langle E_{\rm targ}\right\rangle$ is greatest for low E owing to the strong interaction with the projectile at small impact parameters required to eject the electron. As E increases, less central collisions are able to eject the electron and less energy is transferred to the recoiling target. The recoil

angle tends to be opposite to the projectile scattering, conserving momentum in the collision along with that from the lower-mass but swifter ejected electron, resulting in generally greater $\langle\theta_{\rm targ}\rangle$ as $\langle\theta_{\rm proj}\rangle$ becomes smaller.

All these correlated behaviors result in the variation of the average energy loss, which is largest at low E when the $\langle\theta_{\rm proj}\rangle$ and $\left\langle E_{\rm targ}\right\rangle$ are largest. The energy loss decreases for intermediate E, as the projectile energy loss and the target recoil energy decrease, rising at higher E as the contribution from higher $\langle E_{\rm elec}\rangle$ grows.

Next in level of detail of description of the collision we tabulate (Table 2) the singly differential cross sections corresponding to these average kinematic parameters, namely, $d\sigma/d\theta_{\rm proj}$, $d\sigma/dE_{\rm elec}$, $d\sigma/d\theta_{\rm elec}$, $d\sigma/dE_{\rm targ}$, and $d\sigma/d\theta_{\rm targ}$, denoted for simplicity of notation in the figures and tables below as SDCS($\theta_{\rm proj}$), SDCS($\theta_{\rm elec}$), SDCS($E_{\rm elec}$), SDCS($\theta_{\rm targ}$), and SDCS($E_{\rm targ}$), and the energy loss as a function of $\theta_{\rm proj}$.

A transport simulation may sample from these distributions to obtain event-by-event values of $\theta_{\rm proj}$, $E_{\rm elec}$, $\theta_{\rm elec}$, $E_{\rm targ}$, $\theta_{\rm targ}$, and the energy loss as a function of $\theta_{\rm proj}$, yielding the same average values as given in Table 1 but reflecting the full distribution of these parameters of the collision. As noted above, for the lowest impact energies, with the smallest number of events from the CTMC calculations, we have too few counts to report an integral or differential cross section. For impact energies within this range a simulation would use the extrapolated average kinematic parameters in the lack of a tabulated SDCS.

We note that when the integral cross section is normalized to agree with the recommended value, the same normalization factor is applied to the differential cross sections so that they integrate to the same value for consistency in any transport simulation. The normalization does not change the "shape" of the differential cross section, so this process can degrade the physical correctness of the differential cross section. However, as the comparison with the existing measurements shows for 20–100 keV, and, as described below, as calculation of transport-related quantities dependent on both the integral and differential cross section shows, this degradation is not significant.

Benchmarks exist for the calculations of SDCS($E_{\rm elec}$) and SDCS($\theta_{\rm elec}$) from the measurements by Kerby et al. (1995), as displayed in Figures 6 and 7, respectively. For the four impact energies considered by the experiments (20, 48, 67, and 95 keV, compared to the present results at 20, 50, 75, and 100 keV), very good agreement is noted for SDCS($E_{\rm elec}$) and for SDCS($\theta_{\rm elec}$) except at very large ejection angles. Examples of the present results for all the SDCS are illustrated in Figure 8 for energies spanning the range considered (3, 30, 300, 3000 keV).

At the final level of detail considered here, a subset of the many DDCS that could be defined reflecting the correlation of $E_{\rm proj}$, $\theta_{\rm proj}$, $E_{\rm elec}$, $\theta_{\rm elec}$, $E_{\rm targ}$, and $\theta_{\rm targ}$ are made available via doi:10.7910/DVN/GN5SKT. With the likelihood that a simulation would begin the chain of transport events by considering the scattering of the projectile (and then the electron loss, and then emission and recoil of the electron and target, respectively, if the reaction that takes place is ionization), we have selected four DDCS that would therefore be of greatest relevance.

Table 3
Present Recommended Integral Cross Section (as Described in the Text) for Ionization or Stripping and Simultaneous Ionization and Stripping for H + H

Energy (keV)	$\sigma_{\rm ion}$ (cm^2)	$\sigma_{\rm sim}$ (cm^2)
1.36E–02	1.00E–99	…
2.00E–02	1.00E–24	…
2.72E–02	…	1.00E–99
3.00E–02	8.00E–22	2.02E–28
5.00E–02	2.00E–20	1.26E–25
7.00E–02	7.00E–20	1.55E–24
1.00E–01	2.60E–19	2.13E–23
2.00E–01	8.68E–19	2.37E–22
3.00E–01	1.52E–18	7.34E–22
5.00E–01	3.27E–18	3.37E–21
7.00E–01	6.70E–18	1.42E–20
1.00E+00	9.39E–18	4.58E–20
2.00E+00	1.67E–17	1.62E–19
3.00E+00	2.25E–17	3.56E–19
5.00E+00	3.62E–17	8.70E–19
7.00E+00	4.60E–17	1.47E–18
1.00E+01	6.89E–17	3.00E–18
1.20E+01	8.42E–17	3.10E–18
1.40E+01	9.32E–17	3.90E–18
1.60E+01	9.94E–17	4.70E–18
2.00E+01	1.05E–16	7.64E–18
3.00E+01	9.72E–17	7.22E–18
5.00E+01	8.53E–17	6.50E–18
7.00E+01	7.14E–17	5.60E–18
1.00E+02	5.70E–17	4.19E–18
2.00E+02	3.58E–17	1.77E–18
3.00E+02	2.53E–17	1.21E–18
5.00E+02	1.76E–17	6.12E–19
7.00E+02	1.36E–17	3.90E–19
1.00E+03	1.03E–17	2.30E–19
2.00E+03	5.82E–18	7.32E–20
3.00E+03	4.09E–18	3.61E–20
5.00E+03	2.57E–18	1.41E–20
7.00E+03	1.88E–18	7.55E–21
1.00E+04	1.35E–18	3.93E–21

(This table is available in its entirety in machine-readable form.)

4. Ionization and Stripping in H + H

The process of charge transfer ($H^+ + H \rightarrow H + H^+$) leads to a fast neutral, and so here we consider the processes of ionization by H impact (target ionization) and stripping of H by H (projectile ionization). Owing to the symmetry of the collision system, the integral cross section for both processes is identical, but the differential cross sections are not, particularly the SDCS($E_{\rm elec}$) and SDCS($\theta_{\rm elec}$) because in stripping the electron is emitted in the moving frame of the projectile.

For ionization, CTMC calculations proceed largely as for $H^+ + H$ but with a neutral potential (Schultz & Reinhold 1998) representing H impact. Again we employ rCTMC for $E \leqslant 200$ keV and pCTMC for $E \geqslant 300$ keV. Since for the neutral-particle impact there is no long-range Coulomb field of the projectile, there is no B1C for H + H. For stripping, we place the electron on the projectile and use the neutral potential to represent the target–electron and target–projectile nucleus interactions.

In contrast to ionization in $H^+ + H$, there are much fewer experimental and theoretical data for ionization and stripping in H + H, and no recommended or evaluated integral cross

Table 4
Integral Cross Section (Denoted "TCS" for Total Cross Section) along with the Average Values of the Kinematic Parameters of the Collision for Ionization in H + H as a Function of Laboratory Collision Energy from Ionization Threshold to 10 MeV

Energy (keV)	TCS (cm^2)	$\langle E_{loss}^{ioniz} \rangle$ (eV)	$\langle \theta_{proj} \rangle$ (deg)	$\langle E_{elec} \rangle$ (eV)	$\langle \theta_{elec} \rangle$ (deg)	$\langle E_{targ} \rangle$ (eV)	$\langle \theta_{targ} \rangle$ (deg)
1.36E-02	1.00E-99	1.65E+01	6.04E+00	2.78E+00	8.65E+01	1.56E+00	1.11E+01
2.00E-02	1.00E-24	2.60E+01	8.28E+00	1.19E+01	8.89E+01	2.25E+00	1.87E+01
3.00E-02	8.00E-22	2.67E+01	7.32E+00	1.24E+01	8.86E+01	2.17E+00	2.35E+01
5.00E-02	2.00E-20	2.67E+01	5.91E+00	1.23E+01	8.71E+01	1.90E+00	2.96E+01
7.00E-02	7.00E-20	2.66E+01	4.89E+00	1.20E+01	8.70E+01	1.85E+00	3.26E+01
1.00E-01	2.60E-19	2.65E+01	3.96E+00	1.18E+01	8.57E+01	1.90E+00	3.50E+01
2.00E-01	8.68E-19	2.58E+01	2.64E+00	1.10E+01	8.35E+01	2.03E+00	3.91E+01
3.00E-01	1.52E-18	2.50E+01	2.19E+00	9.98E+00	8.04E+01	2.20E+00	4.26E+01
5.00E-01	3.27E-18	2.28E+01	1.74E+00	7.71E+00	7.48E+01	2.36E+00	4.83E+01
7.00E-01	6.70E-18	2.09E+01	1.37E+00	5.96E+00	7.12E+01	2.15E+00	5.12E+01
1.00E+00	9.39E-18	1.92E+01	9.82E-01	4.53E+00	6.74E+01	1.69E+00	5.24E+01
2.00E+00	1.67E-17	1.80E+01	4.61E-01	3.85E+00	5.90E+01	9.15E-01	5.19E+01
3.00E+00	2.25E-17	1.84E+01	2.96E-01	4.44E+00	5.50E+01	6.10E-01	5.18E+01
5.00E+00	3.62E-17	2.00E+01	1.79E-01	6.16E+00	5.06E+01	3.97E-01	5.29E+01
7.00E+00	4.60E-17	2.18E+01	1.32E-01	7.98E+00	4.74E+01	2.98E-01	5.47E+01
1.00E+01	6.89E-17	2.44E+01	9.85E-02	1.07E+01	4.40E+01	2.32E-01	5.76E+01
2.00E+01	1.05E-16	3.23E+01	5.95E-02	1.86E+01	4.10E+01	1.55E-01	6.65E+01
3.00E+01	9.72E-17	3.82E+01	4.58E-02	2.45E+01	4.29E+01	1.20E-01	7.26E+01
5.00E+01	8.53E-17	4.59E+01	3.44E-02	3.22E+01	4.91E+01	9.37E-02	7.89E+01
7.00E+01	7.14E-17	5.03E+01	2.88E-02	3.66E+01	5.42E+01	8.00E-02	8.17E+01
1.00E+02	5.70E-17	5.39E+01	2.40E-02	4.03E+01	5.96E+01	6.72E-02	8.39E+01
2.00E+02	3.58E-17	5.84E+01	1.69E-02	4.48E+01	6.84E+01	5.15E-02	8.68E+01
3.00E+02	2.53E-17	6.37E+01	1.44E-02	5.00E+01	7.10E+01	4.99E-02	8.85E+01
5.00E+02	1.76E-17	6.53E+01	1.09E-02	5.16E+01	7.54E+01	4.29E-02	8.93E+01
7.00E+02	1.36E-17	6.62E+01	9.11E-03	5.25E+01	7.78E+01	5.43E-02	9.08E+01
1.00E+03	1.03E-17	6.71E+01	7.46E-03	5.34E+01	7.97E+01	4.51E-02	9.14E+01
2.00E+03	5.82E-18	6.92E+01	5.10E-03	5.56E+01	8.27E+01	4.87E-02	9.12E+01
3.00E+03	4.09E-18	7.10E+01	4.10E-03	5.73E+01	8.40E+01	3.64E-02	9.09E+01
5.00E+03	2.57E-18	7.35E+01	3.13E-03	5.99E+01	8.53E+01	2.46E-02	9.05E+01
7.00E+03	1.88E-18	7.56E+01	2.62E-03	6.19E+01	8.60E+01	2.36E-02	9.03E+01
1.00E+04	1.35E-18	7.76E+01	2.17E-03	6.38E+01	8.66E+01	2.21E-02	9.02E+01

(This table is available in its entirety in machine-readable form.)

section. Three sets of measurements exist (McClure 1968; Hill et al. 1979; Gealy & Van Zyl 1987), as shown in Figure 9 for the impact energy range around the maximum of the cross section, compared with previous theoretical calculations (Soon 1992; Ovchinnikov et al. 2017).

Since, as for $H^+ + H$, we normalize the present CTMC integral cross sections to the best available estimate, we have created a recommended curve by selecting points from these data as follows: in the absence of any other data to consider, we have used the curve from Soon (1992) from the ionization threshold to 600 eV, joined this smoothly to the advanced adiabatic method results of Ovchinnikov et al. (2017) that are valid in the lower-energy regime, picked up a selection of data points that form a relatively smooth curve from the measurements of Hill et al. (1979) (confirmed by the trend and magnitude of those from Gealy & Van Zyl 1987) from 7 to 20 keV, continued using the measurements from McClure (1968), then used the curve from Soon (1992) from 30 to 100 keV, and adopted the CTMC results from 100 keV to 10 MeV. This recommended curve is shown in Figure 10, along with the present CTMC results, and tabulated in Table 3.

Tables 4 and 6 give the integral cross section (normalized to the present recommended curve) and average values of the kinematic parameters for H + H ionization and stripping, respectively. The corresponding singly differential cross sections are given in Tables 5 and 7, respectively. The behavior of the kinematic parameters as a function of impact energy is illustrated in Figure 11. For ionization they display generally the same behavior as those for $H^+ + H$ with some variation particularly at low impact energy owing to (i) the difference in ionization probability for the neutral projectile and (ii) the fact that charge transfer is highly probable for proton impact and negative ion formation considerably smaller for the neutral impact. The other significant difference is the change in the behavior for stripping compared to ionization in H + H, primarily at high impact energies owing to the greater kinetic energy, and forward motion, of the electron ejected from the swift projectile. The full distribution of the particle energies and scattering/emission/recoil angles is illustrated in Figures 12 and 13 via the SDCS for ionization and stripping, respectively. The DDCS for ionization and stripping are made available via doi:10.7910/DVN/GN5SKT.

5. Simultaneous Ionization and Stripping in H + H

For completeness of the present data set regarding electron ejection in H + H collisions, we include here an estimate of the simultaneous ionization and stripping integral cross section, σ_{sim}. As demonstrated below, it is about 20 times smaller at the peak of the cross section at ~20 keV than the ionization (or stripping) integral cross section, and about 200 times smaller at 10 MeV. In addition, with a threshold energy of twice the

Table 5
SDCS and Projectile Energy Loss as Functions of θ_{proj}, E_{elec}, θ_{elec}, E_{targ}, and θ_{targ} for Ionization in H Impact on H

E_{imp} (keV)	θ_{proj} (deg)	$E_{loss}(\theta_{proj})$ (eV)	SDCS(θ_{proj}) (cm^2 sr^{-1})	E_{elec} (eV)	SDCS(E_{elec}) (cm^2 eV^{-1})	θ_{elec} (deg)	SDCS(θ_{elec}) (cm^2 sr^{-1})	E_{targ} (eV)	SDCS(E_{targ}) (cm^2 eV^{-1})	θ_{targ} (deg)	SDCS(θ_{elec}) (cm^2 sr^{-1})
2.00E-02	1.50E-01	2.38E+01	6.21E-23	3.00E-01	1.24E-25	1.10E+01	6.56E-26	3.00E-01	7.68E-26	5.00E-01	1.74E-23
⋯	3.00E-01	2.16E+01	3.32E-23	7.50E-01	4.73E-26	1.50E+01	6.93E-26	7.50E-01	2.58E-25	7.00E-01	1.09E-23
⋯	5.00E-01	2.25E+01	3.39E-23	3.00E+00	1.82E-26	1.70E+01	6.54E-26	3.00E+00	2.03E-25	9.00E-01	1.36E-23
⋯	7.00E-01	2.51E+01	3.64E-23	6.25E+00	4.27E-26	1.90E+01	6.06E-26	6.25E+00	7.71E-27	1.50E+00	7.45E-24
⋯	9.00E-01	2.51E+01	3.19E-23	8.75E+00	6.59E-26	2.25E+01	5.70E-26	8.75E+00	2.50E-27	2.50E+00	5.25E-24
⋯	1.50E+00	2.49E+01	2.12E-23	1.25E+01	6.31E-26	2.75E+01	6.82E-26	1.25E+01	5.19E-28	3.50E+00	3.30E-24
⋯	2.50E+00	2.54E+01	1.10E-23	1.75E+01	2.85E-26	3.25E+01	7.07E-26	⋯	⋯	4.50E+00	2.66E-24
⋯	3.50E+00	2.48E+01	9.40E-24	2.50E+01	9.70E-27	3.75E+01	7.81E-26	⋯	⋯	5.50E+00	2.01E-24
⋯	4.50E+00	2.55E+01	7.74E-24	4.00E+01	1.12E-27	4.25E+01	6.99E-26	⋯	⋯	6.50E+00	2.17E-24
⋯	5.50E+00	2.56E+01	7.28E-24	⋯	⋯	4.75E+01	7.33E-26	⋯	⋯	7.50E+00	1.46E-24

(This table is available in its entirety in machine-readable form.)

Table 6
Integral Cross Section (Denoted "TCS" for Total Cross Section) along with the Average Values of the Kinematic Parameters of the Collision for Stripping in H + H as a Function of Laboratory Collision Energy from Ionization Threshold to 10 MeV

Energy (keV)	TCS (cm^2)	$\langle E_{loss}^{ioniz} \rangle$ (eV)	$\langle \theta_{proj} \rangle$ (deg)	$\langle E_{elec} \rangle$ (eV)	$\langle \theta_{elec} \rangle$ (deg)	$\langle E_{targ} \rangle$ (eV)	$\langle \theta_{targ} \rangle$ (deg)
1.36E-02	1.00E-99	2.01E+01	6.40E+00	6.37E+00	8.67E+01	1.57E+00	1.76E+01
2.00E-02	1.00E-24	2.54E+01	8.03E+00	1.13E+01	8.92E+01	2.17E+00	1.93E+01
3.00E-02	8.00E-22	2.60E+01	7.14E+00	1.17E+01	9.02E+01	2.08E+00	2.42E+01
5.00E-02	2.00E-20	2.64E+01	5.82E+00	1.17E+01	8.95E+01	1.86E+00	3.02E+01
7.00E-02	7.00E-20	2.65E+01	4.90E+00	1.15E+01	8.90E+01	1.86E+00	3.32E+01
1.00E-01	2.60E-19	2.65E+01	3.85E+00	1.19E+01	8.92E+01	1.81E+00	3.53E+01
2.00E-01	8.68E-19	2.59E+01	2.55E+00	1.10E+01	8.90E+01	1.96E+00	3.92E+01
3.00E-01	1.52E-18	2.49E+01	2.11E+00	9.94E+00	8.89E+01	2.12E+00	4.24E+01
5.00E-01	3.27E-18	2.29E+01	1.70E+00	7.66E+00	8.71E+01	2.32E+00	4.78E+01
7.00E-01	6.70E-18	2.10E+01	1.35E+00	5.86E+00	8.42E+01	2.13E+00	5.04E+01
1.00E+00	9.39E-18	1.92E+01	9.67E-01	4.35E+00	8.14E+01	1.71E+00	5.10E+01
2.00E+00	1.67E-17	1.80E+01	4.53E-01	3.27E+00	8.04E+01	9.22E-01	4.86E+01
3.00E+00	2.25E-17	1.83E+01	2.89E-01	3.45E+00	8.10E+01	6.15E-01	4.68E+01
5.00E+00	3.62E-17	1.99E+01	1.73E-01	4.28E+00	8.27E+01	4.05E-01	4.52E+01
7.00E+00	4.60E-17	2.17E+01	1.26E-01	5.11E+00	8.44E+01	3.16E-01	4.45E+01
1.00E+01	6.89E-17	2.44E+01	9.28E-02	6.23E+00	8.61E+01	2.43E-01	4.40E+01
2.00E+01	1.05E-16	3.22E+01	5.34E-02	9.86E+00	8.53E+01	1.69E-01	4.43E+01
3.00E+01	9.72E-17	3.81E+01	3.93E-02	1.39E+01	7.96E+01	1.34E-01	4.60E+01
5.00E+01	8.53E-17	4.58E+01	2.72E-02	2.29E+01	6.72E+01	1.14E-01	5.02E+01
7.00E+01	7.14E-17	5.01E+01	2.16E-02	3.28E+01	5.72E+01	8.53E-02	5.40E+01
1.00E+02	5.70E-17	5.38E+01	1.70E-02	4.81E+01	4.69E+01	9.08E-02	5.83E+01
2.00E+02	3.58E-17	5.82E+01	1.09E-02	1.01E+02	3.07E+01	6.58E-02	6.62E+01
3.00E+02	2.53E-17	6.32E+01	8.64E-03	1.53E+02	2.52E+01	7.73E-02	6.83E+01
5.00E+02	1.76E-17	6.47E+01	6.82E-03	2.62E+02	1.85E+01	6.69E-02	7.28E+01
7.00E+02	1.36E-17	6.55E+01	5.69E-03	3.71E+02	1.52E+01	6.95E-02	7.53E+01
1.00E+03	1.03E-17	6.63E+01	4.72E-03	5.34E+02	1.24E+01	6.46E-02	7.74E+01
2.00E+03	5.82E-18	6.82E+01	3.28E-03	1.08E+03	8.40E+00	8.25E-02	8.08E+01
3.00E+03	4.09E-18	6.96E+01	2.65E-03	1.62E+03	6.77E+00	8.84E-02	8.24E+01
5.00E+03	2.57E-18	7.20E+01	2.03E-03	2.71E+03	5.19E+00	5.01E-02	8.40E+01
7.00E+03	1.88E-18	7.37E+01	1.70E-03	3.80E+03	4.38E+00	4.08E-02	8.49E+01
1.00E+04	1.35E-18	7.54E+01	1.42E-03	5.43E+03	3.66E+00	5.77E-02	8.57E+01

(This table is available in its entirety in machine-readable form.)

ionization potential of H (27.2 eV), σ_{sim} drops much faster at low impact energies.

A highly accurate description of this process would require a full two-center, two-electron quantum mechanical treatment but may be estimated using the present calculations by employing the independent electron model (see, e.g., McGuire & Weaver 1977), expressing the two-electron transition probability in terms of a binomial distribution of the one-electron transition probabilities. Though derived for transitions on a single center, we adopt the same formula for the probability as a function of impact parameter (b) for simultaneous ionization (target-centered transition) and stripping (projectile-centered transition) as McGuire & Weaver (1977) derive for double ionization (target-centered transition), namely,

$$P_{sim}(b) = P_{ionization}(b) \times P_{stripping}(b). \quad (4)$$

Forming this product from the present rCTMC and pCTMC calculations, we obtain σ_{sim} as usual in the CTMC method, that is, via

$$\sigma_{sim} = \pi\, a_o^2\, b_{max}^2 \sum_{b=0}^{b=b_{max}} P_{sim}(b), \quad (5)$$

where a_o is the Bohr radius (the unit of length in atomic units, 0.529×10^{-8} cm^2) and b_{max} is the largest impact parameter, beyond which the probability is zero.

For ionization or stripping, despite the significant difference in distribution of $P_{ionization}(b)$ or $P_{stripping}(b)$ for rCTMC and pCTMC, the resulting integral cross sections largely agree for impact energies between about 20 and 200 keV, facilitating their smooth connection as described above. Taking the product of these probabilities accentuates the difference in the distributions as a function of b, and therefore for σ_{sim} the integral cross sections from rCTMC and pCTMC do not smoothly connect. We therefore join them by taking rCTMC below 1 keV and pCTMC above 200 keV, with a smooth combination of the two for intermediate values. The values obtained in this way for σ_{sim} are tabulated in Table 3.

In a transport simulation including simultaneous ionization and stripping, the SDCS, DDCS, and average parameters may be estimated via appropriate combinations of the corresponding data for ionization and stripping at the level of approximation of independent consideration of the processes, as follows:

1. $\langle E_{elec} \rangle$ or $\langle \theta_{elec} \rangle$—use the average values for ionization to determine the energy or ejection angle for the target electron and the average values for stripping to determine the energy or ejection angle for the projectile electron.

Table 7
SDCS and Projectile Energy Loss as Functions of θ_{proj}, E_{elec}, θ_{elec}, E_{targ}, and θ_{targ} for Stripping in H Impact on H

E_{imp} (keV)	θ_{proj} (deg)	$E_{loss}(\theta_{proj})$ (eV)	SDCS(θ_{proj}) (cm^2 sr^{-1})	E_{elec} (eV)	SDCS(E_{elec}) (cm^2 eV^{-1})	θ_{elec} (deg)	SDCS(θ_{elec}) (cm^2 sr^{-1})	E_{targ} (eV)	SDCS(E_{targ}) (cm^2 eV^{-1})	θ_{targ} (deg)	SDCS(θ_{elec}) (cm^2 sr^{-1})
2.00E-02	1.50E-01	2.60E+01	9.76E-23	3.00E-01	1.70E-25	9.50E+00	1.03E-25	3.00E-01	9.11E-26	7.00E-01	8.72E-24
⋯	3.00E-01	2.76E+01	7.93E-23	7.50E-01	4.11E-26	1.10E+01	3.91E-26	7.50E-01	3.28E-25	9.00E-01	7.46E-24
⋯	5.00E-01	2.61E+01	6.59E-23	3.00E+00	2.64E-26	1.30E+01	4.26E-26	3.00E+00	1.92E-25	1.50E+00	4.64E-24
⋯	7.00E-01	2.39E+01	4.88E-23	6.25E+00	7.25E-26	1.50E+01	5.76E-26	6.25E+00	8.41E-27	2.50E+00	5.18E-24
⋯	9.00E-01	2.40E+01	3.86E-23	8.75E+00	7.68E-26	1.70E+01	8.01E-26	8.75E+00	2.62E-27	3.50E+00	4.60E-24
⋯	1.50E+00	2.46E+01	1.93E-23	1.25E+01	3.95E-26	1.90E+01	2.94E-26	1.25E+01	4.67E-28	4.50E+00	2.71E-24
⋯	2.50E+00	2.43E+01	1.42E-23	1.75E+01	2.02E-26	2.25E+01	6.12E-26	⋯	⋯	5.50E+00	2.16E-24
⋯	3.50E+00	2.56E+01	1.01E-23	2.50E+01	8.17E-27	2.75E+01	6.37E-26	⋯	⋯	6.50E+00	1.96E-24
⋯	4.50E+00	2.35E+01	7.46E-24	4.00E+01	2.10E-27	3.25E+01	5.23E-26	⋯	⋯	7.50E+00	1.93E-24
⋯	5.50E+00	2.57E+01	6.75E-24	6.00E+01	2.69E-28	3.75E+01	7.35E-26	⋯	⋯	8.50E+00	1.50E-24

(This table is available in its entirety in machine-readable form.)

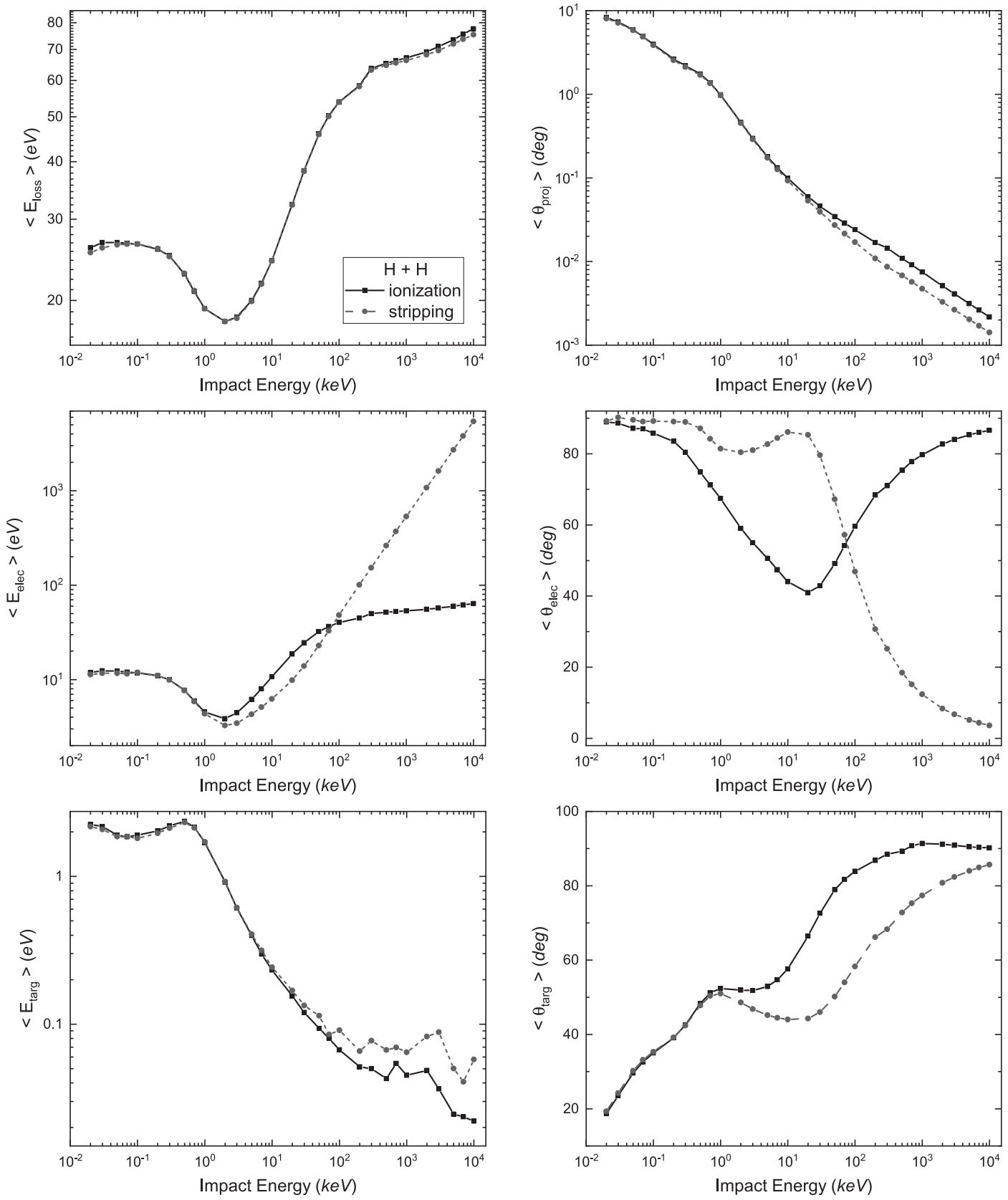

Figure 11. Behavior as a function of laboratory impact energy of the average kinematic parameters for ionization (solid curves) and stripping (dashed curves) in H + H collisions.

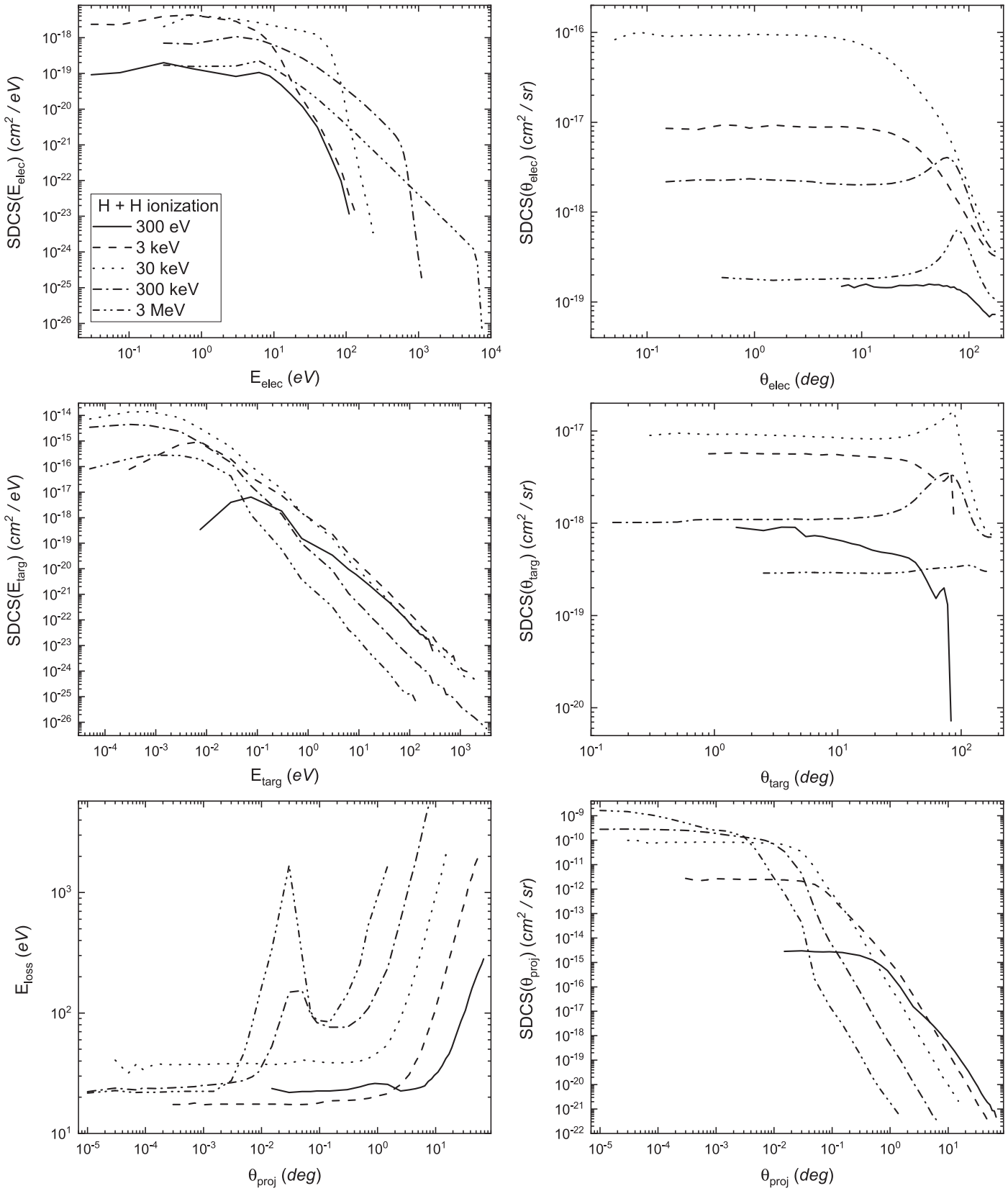

Figure 12. Illustration of the SDCS for ionization in H + H for four representative laboratory-frame impact energies.

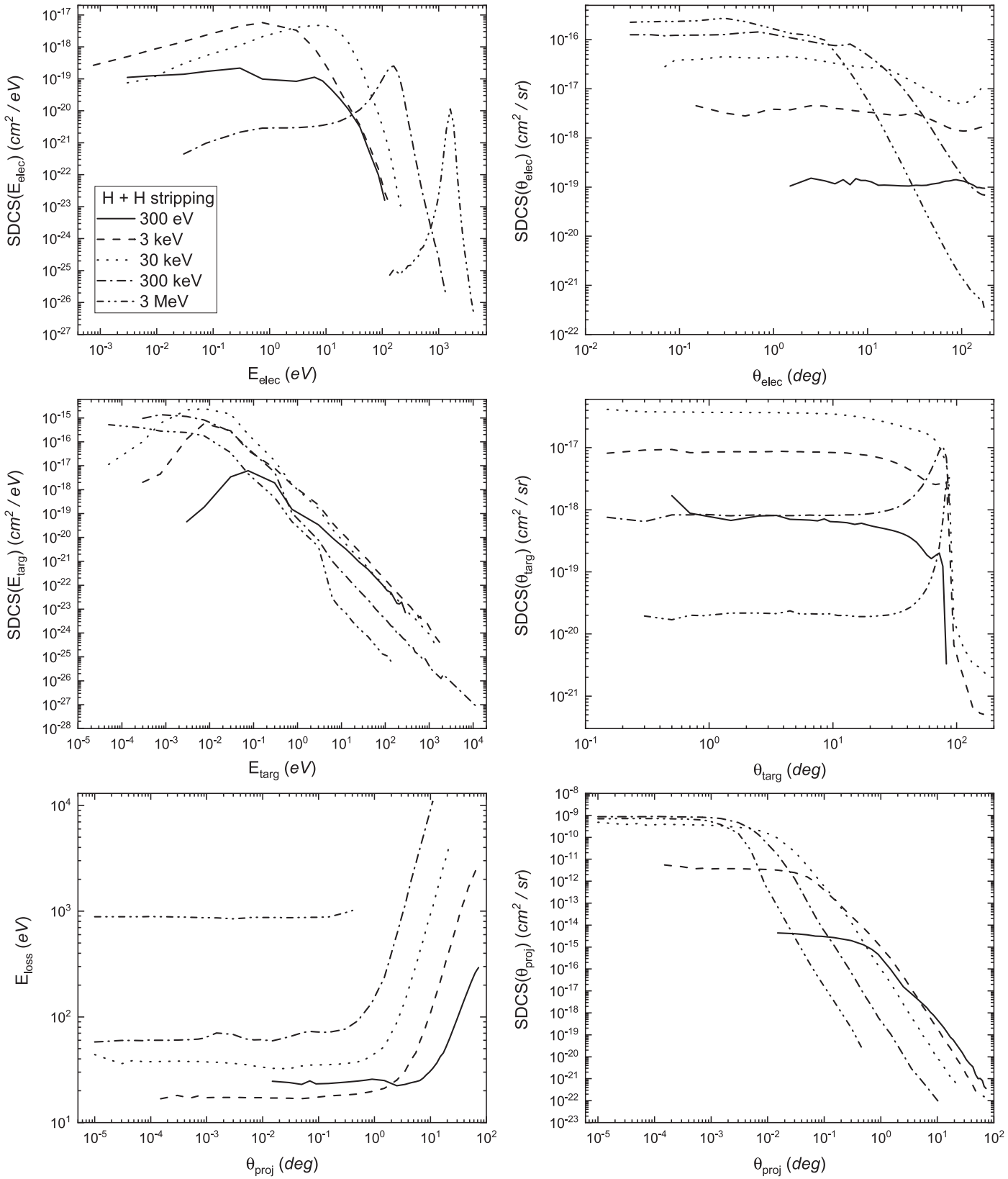

Figure 13. Illustration of the SDCS for stripping in H + H for four representative laboratory-frame impact energies.

2. SDCS(E_{elec}) or SDCS(θ_{elec})—sample the SDCS for ionization to obtain the energy or ejection angle for the target electron and sample the SDCS for stripping to obtain the energy or ejection angle for the projectile electron.
3. $\langle\theta_{proj}\rangle$ or SDCS(θ_{proj})—add the average values of θ_{proj} for ionization and stripping, or sample SDCS(θ_{proj}) for both ionization and stripping and add the resulting sampled values, to approximate the projectile scattering angle.
4. Average value of the energy loss or the energy loss as a function of θ_{proj}—add the average value of energy loss for ionization and stripping, or sample the energy loss as a function of θ_{proj} for ionization and stripping, to approximate the projectile energy loss.
5. $\langle E_{targ}\rangle$, $\langle\theta_{targ}\rangle$, SDCS($E_{targ}$), or SDCS($\theta_{targ}$)—add the average values of E_{targ} or θ_{targ} for ionization and stripping, or sample SDCS(E_{targ}) or SDCS(θ_{targ}) for both ionization and stripping and add the resulting sampled values, to approximate the target energy or recoil angle.
6. DDCS(θ_{proj}, E_{elec}) or DDCS(θ_{proj}, θ_{elec})—sample the DDCS for ionization to obtain the energy or ejection angle for the target electron and projectile scattering angle and sample the DDCS for stripping to obtain the energy or ejection angle for the projectile electron and projectile scattering angle, adding the two projectile scattering angles.
7. DDCS(θ_{proj}, E_{targ}) or DDCS(θ_{proj}, θ_{targ})—sample the DDCS for ionization to obtain the energy or recoil angle for the target and projectile scattering angle and sample the DDCS for stripping to obtain the energy or recoil angle for the target and the projectile scattering angle, adding the two energies or recoil angles for the target and adding the two projectile scattering angles.

6. Summary

In the present work we have calculated, described, and tabulated data for ionization in $H^+ + H$, and for ionization and stripping in $H + H$, over a wide range of impact energies, to help enable more complete modeling of the passage of H^+ and H through hydrogen astrophysical environments. This has been done at three progressively more physically detailed levels to allow users of the data to match the varying needs or goals of their heavy-particle and secondary-electron transport simulations. Toward this end we have accounted for the best available benchmarks for our calculations. The comprehensiveness required for modeling necessitates inclusion of data for the full range of impact energies considered even if results for the differential cross sections at the lowest energies cannot be benchmarked in this way or calculated without use of normalization to the total cross section that constrains them.

Coupled with other published, in progress, or future tabulations of data for other reaction channels in H^+, $H + H$, this work has been aimed at providing comprehensive knowledge of the underpinning laboratory astrophysics data required to better understand the dynamics and other properties of these ubiquitous interactions.

In particular, we plan to link all of the data produced into a comprehensive network of elastic and inelastic processes (elastic scattering, target and projectile excitation, target and projectile ionization, and charge transfer) to enable transport simulation of protons and hydrogen propagating through hydrogen. The simulation will enable accurate modeling of the slowing down of these projectiles, their angular scattering, production of excitation throughout the projectile's trajectory and thus emission, rates of neutralization and reionization of protons, and secondary-electron production that seeds further excitation, emission, and reactions. Finally, the resulting transport simulation will allow validation of the underlying data set by producing quantities including the stopping power, ion charge state distribution, and other transport properties that have been measured for comparison.

We describe in the Appendix results of such a calculation of these transport-related quantities that we have performed utilizing preliminary and published data, helping to validate the entire data set, including the present calculations of ionization and stripping in H^+, $H + H$ collisions.

The authors gratefully acknowledge support for this research through NASA's Astrophysics Research and Analysis program via grant No. 80NSSC18K0248.

Appendix
The Charge State Fractions and Stopping Power for $H^{-,0,+}$ + H and H_2 as a Function of Impact Energy

A transport simulation of hydrogen passing through hydrogen, as the present work aims to contribute new data to support, should be capable of describing all quantities of astrophysical interest such as the distribution of excitation along the trajectory of passage, the distribution of electrons ejected, and the charge, energy, and direction change of the incident particle. Wherever possible this large atomic collision and transition data set should be benchmarked through direct comparison with fiducial experiments. However, as stated in the text, more global physical measures are capable of providing an additional check when such benchmarks are not available, as is the case for a large portion of the data for $H^{-,0,+} + H$. Such measures include the charge state fractions, the average charge state, and the stopping power as a function of incident particle energy.

We have recently calculated these transport-related quantities for $H^{-,0,+} + H_2$ (Schultz et al. 2020) as a test of the overall data set encompassing all reaction channels, and we do so here for $H^{-,0,+} + H$ as a similar test. To achieve this, we have completed preliminary calculations of all the reaction channels required for transport simulations for $H^{-,0,+} + H$. Some of these processes have small contributions to the determination of these transport-related quantities but are included in our work because of their importance for aspects of astrophysical modeling (e.g., distribution of excitation, production of H^-, which is a catalyst for other reactions, etc.).

Also of interest is the difference between the probabilities of reactions (related to the integral cross sections for each process), the associated energy losses, and the transport-related quantities for H and H_2. This is of more than academic interest, as data for H_2 are often used as a surrogate for H because laboratory measurements are much more feasible for H_2 than H. As shown in Table 8, the one-, two-, and three-electron transition processes contain significantly different channels in addition to those that H and H_2 share in common, such as elastic scattering, single ionization, and single charge transfer. Owing to their similar ionization potentials, the transport-related quantities for H and H_2 have great similarities in their magnitude and behavior as a function of impact energy despite significant differences in the reaction products and energy losses in some of the channels. This underscores the complementary nature of validating the atomic collision and

Table 8
Processes (Reaction Channels) in H^+, H, and H^- Collisions with H for Energies between About 10 and 10^7 eV and Those Previously Considered for H^+, H, and H^- with H_2 (Schultz et al. 2020)

H^+, H, H^- + H	H^+, H, H^- + H_2
$H^+ + H \rightarrow H^+ + H$ EL[1,2]	$H^+ + H_2 \rightarrow H^+ + H_2$ EL[5]
$H^+ + H \rightarrow H^+ + H^+ + e^-$ SI[3]	$H^+ + H_2 \rightarrow H^+ + X + e^-$ SI[5]
$H^+ + H \rightarrow H^+ + H^*$ EX[4,2]	$H^+ + H_2 \rightarrow H^+ + H^+ + H^+ + 2e^-$ DI[5]
$H^+ + H \rightarrow H^* + H^+$ SC[2]	$H^+ + H_2 \rightarrow H^* + H^+ + H^+ + e^-$ TI[5]
	$H^+ + H_2 \rightarrow H^+ + H_2^*$; X EX[5]
	$H^+ + H_2 \rightarrow H^* + X$ SC[5]
	$H^+ + H_2 \rightarrow H^- + X$ DC[5]
$H + H \rightarrow H + H$ EL[1,2]	$H + H_2 \rightarrow H + H_2$ EL[5]
$H + H \rightarrow H + H$ SE[1,2]	$H + H_2 \rightarrow H + H_2$ EL[5]
$H + H \rightarrow H^* + H^+ + e^-$ SI or SI + PEX[3][a]	$H + H_2 \rightarrow H^+ + X + e^-$ SS or SS + DISS[5]
$H + H \rightarrow H^+ + e^- + H^*$ SS or SS + PEX[3][a]	$H + H_2 \rightarrow H + H^+ + H^+ + 2e^-$ DI[5]
$H + H \rightarrow H^+ + H^+ + 2e^-$ SI or SS[3][a]	$H + H_2 \rightarrow H^- + H^+ + H^+ + e^-$ TI/NI[5]
$H + H \rightarrow H^* + H^*$ TEX or/and PEX[2][a]	$H + H_2 \rightarrow H + H_2^*$; X targ EX[5]
$H + H \rightarrow H^- + H$; $H + H^-$ targ or proj NI[6,2]	$H + H_2 \rightarrow H^* + X$ proj EX[5]
	$H + H_2 \rightarrow H^- + X$ NI[5]
$H^- + H \rightarrow H^- + H$ EL[2]	$H^- + H_2 \rightarrow H^- + H_2$ EL[5]
$H^- + H \rightarrow H^- + H^+ + e^-$ SI[2]	$H^- + H_2 \rightarrow H^- + X + e^-$ SI[5]
$H^- + H \rightarrow H^- + H^*$ EX[2]	$H^- + H_2 \rightarrow H^- + H^+ + H^+ + 2e^-$ DI[5]
$H^- + H \rightarrow H + e^- + H^*$ SS or SS + TEX[2][a]	$H^- + H_2 \rightarrow H^- + H_2^*$; X EX[5]
$H^- + H \rightarrow H^* + e^- + X$ SS + PEX or SS + SI[3] or	$H^- + H_2 \rightarrow H + X$ SS[5]
SS + PEX + TEX or SS + PEX + SI[2]	$H^- + H_2 \rightarrow H^+ + X$ DS[5]
$H^- + H \rightarrow H^+ + 2e^- + H$ DS[2]	
$H^- + H \rightarrow H^+ + 2e^- + X$ DS or DS + TEX or DS + SI[2][a]	

Notes. Abbreviations for the processes are as follows: EL—elastic scattering; SE—spin exchange; SI, DI, TI—single, double, and transfer ionization; TEX, PEX—target and/or projectile excitation; SC, DC—single and double capture; SS, DS—single and double stripping; NI—negative ion formation; DISS—dissociation. "X" stands for any product for collisions with H_2 (e.g., H_2^+, $H^+ + H^+$, H_2^*, H^*, $H + e^-$). References: (1) Schultz et al. 2016; (2) present preliminary calculations; (3) this work; (4) Schultz & Ovchinnikov 2015; (5) Schultz et al. 2020; (6) Ovchinnikov et al. 2017. Results of the preliminary calculations will be included in works for publication in preparation.
[a] Includes two- or three-electron transitions.

transition data set through calculation of the transport-related quantities and, wherever possible, the individual channel integral and differential cross sections and energy-loss behaviors that are needed in detailed astrophysical simulations.

To illustrate broadly this diversity of processes and their relative significance to the stopping power, the top panels of Figure 14 display[3] the product of the integral cross section (σ) and the average energy loss ($\langle \Delta E \rangle$) for the processes given in the table for H and H_2. When weighted by the fractions of each projectile charge state at a given impact energy, this quantity is proportional to the stopping power. The data for H are from the present and previous work as referred to in Table 8, and those for H_2 are from Schultz et al. (2020). All of these data are used to first compute the charge state fractions and average charge state, $\langle q \rangle$ (middle panels of the figure) and then the stopping power (bottom panels). These are calculated as described in Schultz et al. (2020) via a transport simulation using the full data set including the integral and differential cross sections and energy-loss formulae, or simply by use of σ and $\langle \Delta E \rangle$.

Despite the fundamental importance of the charge state fractions as a function of impact energy, there exist almost no measurements of this quantity for these important targets. As demonstrated previously (Schultz et al. 2020), we have obtained good agreement with the measurements summarized by Allison (1958) for H_2. Comparing results for H and H_2, we note the slightly different distribution of the negative ion fraction for the two targets, which influences the convergence to the low-energy limit of the ion fractions, arising from the differences in negative ion formation channels and their behaviors. We also note somewhat different behavior at high energies, characterized, for example, by the difference in the energy at which equal fractions of projectile H^+ and H exist for H_2 (about 62 keV) and H (43 keV), owing to the differences in the dominant charge- and energy-changing channels.

Fortunately, a number of measurements of the stopping power for H_2 exist, and calculations using the data set provided by Schultz et al. (2020) agree well with them, as well as with the most widely used recommended value (from SRIM) and the earlier recommended value from Janni (1982). The SRIM database[4] gives a recommended stopping power as a function

[3] The curves in the top panels of the figure are meant to illustrate the many processes that contribute and the wide range of these contributions to the stopping power. Detailed tables of data containing the cross sections and energy losses will be provided in subsequent publications for these processes. To aid in identifying the curves in the figure presented here, we identify them by the order from largest to smallest along a vertical line at 100 keV. Using the notation given in the table for the processes, and indicating the projectile, for H, this order is H^- SS, H^- SI, H^+ SI, H SI (and equal in magnitude H SS), H^+ TEX, H^- TEX, H^- DS, H^+ SC, H SS-SI, H TEX (and equal in magnitude H PEX), H^- SS-SI, H SS-TEX (and equal in magnitude H SI-PEX), H^- SS-TEX (and equal in magnitude H^- SS-PEX), H^- DS-TEX, H^- DS-SI, H PEX-TEX, H targ NI (and equal in magnitude H proj NI), H EL, H^+ EL, H^- EL, and H SE. For H_2, the order is H^- SS, H^+ SI, H^- SI, H SS, H SI, H^- DS, H^+ SC, H^+ DI, H^- DI, H^+ TEX, H^- TEX, H^+ TI, H DI, H EL, H^- EL (and equal in magnitude H^+ EL), H PEX, H TEX, H NI, H^+ DC, H TI/NI, and H SS/DISS.

[4] http://www.srim.org

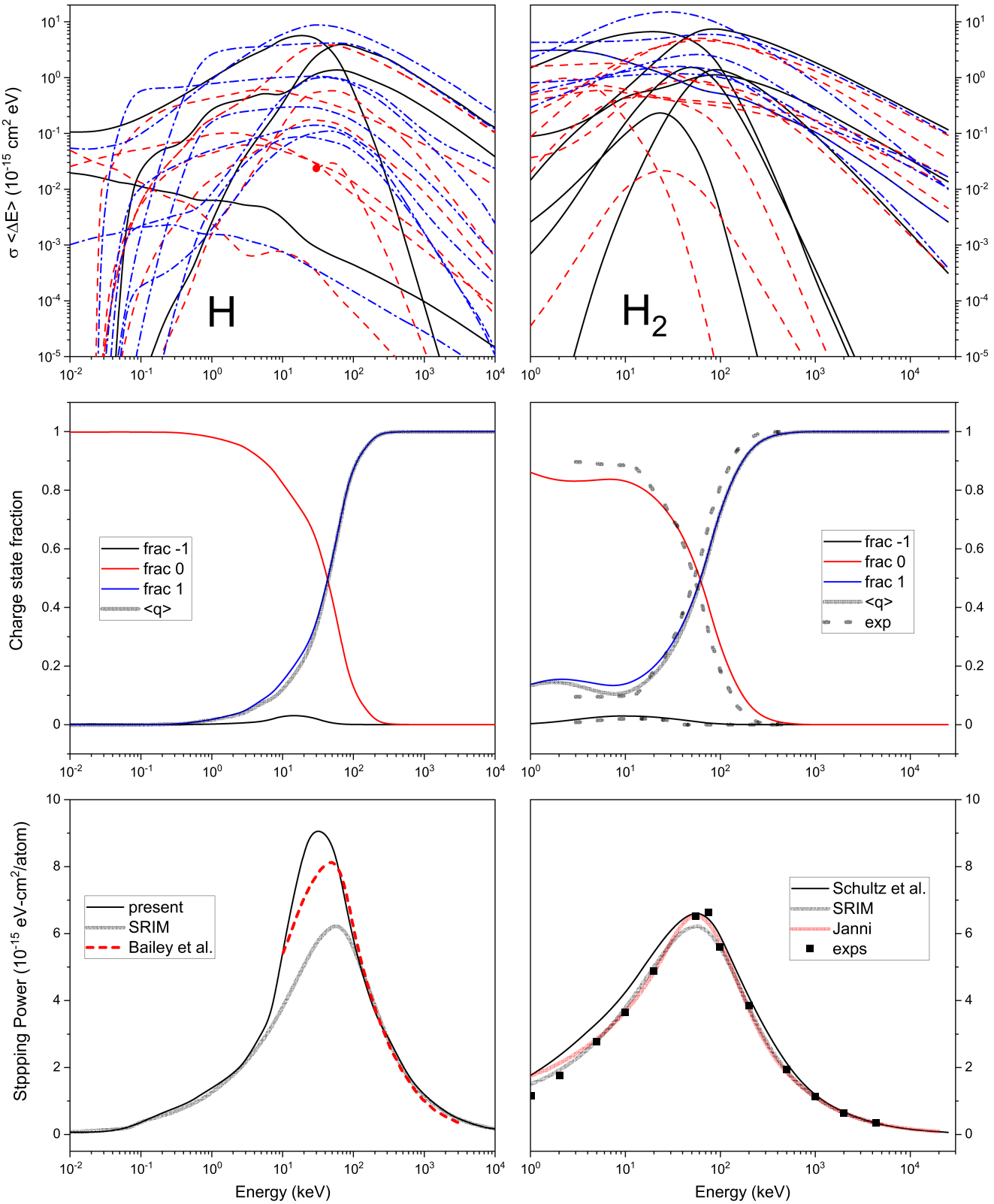

Figure 14. For H (left panels) and H_2 (right panels), the figure compares as a function of impact energy (i) the individual channel contributions to the stopping power (the integral cross section, σ, multiplied by the average energy loss for that process, $\langle \Delta E \rangle$, top panels), (ii) the charge state fractions and average charge state, $\langle q \rangle$ (middle panels), and (iii) the stopping power (bottom panels). The $\sigma\langle \Delta E \rangle$ products are given by black solid lines for H^+ impact, red dashed lines for H impact, and blue dashed-dotted lines for H^- impact. The red filled circle indicates the energy at which the H + H negative ion formation process has a negative $\langle \Delta E \rangle$ (energy gain). The source for the data is as indicated in Table 8. The existing measurements for the charge state fractions for H_2 were summarized by Allison (1958) and are denoted "exp" in the legend, and the measurements summarized here for stopping power for H_2 are referred to in the legend as "exps" and the references are given in Schultz et al. (2020). The other stopping power data displayed are from Schultz et al. (2020), Bailey et al. (2019), Stopping and Range of Ions in Matter (SRIM), and Janni (1982).

of impact energy for H essentially identical to that for H_2, as seen in the figure. Results using the present data for H are in better agreement with recent calculations using a completely independent theoretical approach (Bailey et al. 2019).

Our results are about 10% larger at the peak, differing from their value of $\sigma\langle\Delta E\rangle$ at intermediate energies largely owing to the difference in the H + H ionization channel (about two-thirds of the difference) and secondarily due to the inclusion of the multielectron transition processes given in Table 8 (about one-third of the difference). The present data adopt the magnitude of the integral cross section for this process given by the consensus of the measurements in this energy range (10–30 keV), joining with our previous calculations for H + H ionization (Ovchinnikov et al. 2017) and the measurements below this and with our present calculations and the measurements above (see Figures 9 and 10 in the main text of the present paper).

Therefore, the value of comparison of transport-related quantities, such as the charge state fractions and stopping power, with measurements, with results of other work, and with other closely related collision systems (i.e., H and H_2) indeed provides an important assessment of the entire data set when benchmarks do not exist for all of the most significant channels (i.e., largest contributions to the stopping power) or otherwise important channels (e.g., unique process pathways of astrophysical interest).

References

Abdurakhmanov, I. B., Alladustov, S. U., Bailey, J. J., Kadyrov, A. S., & Bray, I. 2018, PPCF, 60, 095009
Abrines, R., & Percival, I. C. 1966, PPS, 88, 861
Allison, S. K. 1958, RvMP, 30, 1137
Bailey, J. J., Abdurakhmanov, I. B., Kadyrov, A. S., Bray, I., & Mukhamedzhanov, A. M. 2019, PhRvA, 99, 042701
Cohen, J. S. 1985, JPhB, 18, 1759
Gealy, M. W., & Van Zyl, B. 1987, PhRvA, 36, 3100
Hardie, D. J. W., & Olson, R. E. 1983, JPhB, 16, 1983
Hill, J., Geddes, J., & Gilbody, H. B. 1979, JPhB, 12, 3341
Houston, S. J., Cravens, T. E., Schultz, D. R., et al. 2020, JGRA, 125, e27007
Houston, S. J., Ozak, N., Young, J., Cravens, T. E., & Schultz, D. R. 2018, JGRA, 123, 2257
Hsu, Y. Y., Gealy, M. W., Kerby, G. W. I., et al. 1996, PhRvA, 53, 303
Hunter, H. T., Kirkpatrick, M. I., Álvarez, I., et al. 1990, Atomic Data for Fusion: Collisions of H, H_2, He and Li Atoms and Ions with Atoms and Molecules, Oak Ridge National Laboratory, https://inis.iaea.org/collection/NCLCollectionStore/_Public/22/011/22011031.pdf?r=1&r=1
Janev, R. K., & Smith, J. J. 1993, Atomic and Plasma–Material Interaction Data for Fusion No. 4, IAEA, https://www.iaea.org/publications/1839/atomic-and-plasma-material-interaction-data-for-fusion
Janni, J. F. 1982, ADNDT, 27, 147
Kerby, G. W. I., Gealy, M. W., Hsu, Y. Y., et al. 1995, PhRvA, 51, 2256
Kołakowska, A., Pindzola, M. S., & Schultz, D. R. 1999, PhRvA, 59, 3588
McClure, G. W. 1968, PhRv, 166, 22
McGuire, J. H., & Weaver, L. 1977, PhRvA, 16, 41
Olson, R. E., & Salop, A. 1977, PhRvA, 16, 531
Ovchinnikov, S. Y., Kamyshkov, Y., Zaman, T., & Schultz, D. R. 2017, JPhB, 50, 085204
Ozak, N., Cravens, T. E., & Schultz, D. R. 2013, GeoRL, 40, 4144
Reinhold, C. O., & Bürgdorfer, J. 1993, JPhB, 26, 3101
Reinhold, C. O., Schultz, D. R., & Olson, R. E. 1991, NIMPB, 56, 271
Sataka, M., Imai, M., Yamazaki, Y., et al. 1994, JPhB, 27, L171
Schultz, D., Gharibnejad, H., Cravens, T., & Houston, S. 2020, ADNDT, 132, 101307
Schultz, D., & Reinhold, C. 1998, CoPhC, 114, 342
Schultz, D. R., Gharibnejad, H., Cravens, T. E., & Houston, S. J. 2019, ADNDT, 126, 1
Schultz, D. R., & Ovchinnikov, S. Y. 2015, JPhCS, 576, 012008
Schultz, D. R., Ovchinnikov, S. Y., Stancil, P. C., & Zaman, T. 2016, JPhB, 49, 084004
Schultz, D. R., Ozak, N., Cravens, T. E., & Gharibnejad, H. 2017, ADNDT, 113, 1
Schultz, D. R., & Reinhold, C. O. 1994, PhRvA, 50, 2390
Shah, M. B., Elliott, D. S., & Gilbody, H. B. 1987, JPhB, 20, 2481
Shah, M. B., Geddes, J., McLaughlin, B. M., & Gilbody, H. B. 1998, JPhB, 31, L757
Shah, M. B., & Gilbody, H. B. 1981, JPhB, 14, 2361
Sidky, E. Y., & Lin, C. D. 2001, PhRvA, 65, 012711
Soon, W. H. 1992, ApJ, 394, 717
Toburen, L. H., Dubois, R. D., Reinhold, C. O., Schultz, D. R., & Olson, R. E. 1990, PhRvA, 42, 5338
Toburen, L. H., McLawhorn, S. L., McLawhorn, R. A., et al. 2006, Radiat. Prot. Dosim., 122, 22
Toshima, N. 1999, PhRvA, 59, 1981
Winter, T. G. 2009, PhRvA, 80, 032701